MARRYING TOPOGRAPHY AND TIDES; A HIGH RESOLUTION TIDAL DATUM AND INTERTIDAL ZONE ELEVATION MODEL FOR IMPROVED DETERMINATION OF SHORT TERM SEA LEVEL RISE IMPACTS IN FLORIDA BAYS

By

NICHOLAS DIGRUTTOLO

A THESIS PRESENTED TO THE GRADUATE SCHOOL
OF THE UNIVERSITY OF FLORIDA IN PARTIAL FULFILLMENT
OF THE REQUIREMENTS FOR THE DEGREE OF
MASTER OF SCIENCE

UNIVERSITY OF FLORIDA

2010

© 2010 Nicholas DiGruttolo

To my wife, Laura, who encouraged me to continue my education

ACKNOWLEDGMENTS

I thank Dr. Ahmed Mohamed for dedicating so much of his time to help me learn about the wide array of technology employed in this study. Thanks to Dr. Grenville Barnes for pushing me to broaden my study beyond measurements and accuracy into policy and law and thanks to Dr. Bob Swett for his direction in building my research abilities and introduction to Sea Grant.

I would also like to acknowledge the contributions of Adam Benjamin, Kuei-tsung (Philips) Shih, Will Dueease, and Apostolos (Tolee) Mamatas, graduate students at the University of Florida, Dr. Valeriy Yarmola of DataGrid International Inc., www.datagrid-international.com, Walter Volkmann of Micro Aerial Projects LLC, www.microdronesamerica.com, and Northrop Grumman Systems Corporation, 3001 International Business Unit, www.northropgrumman.com, in software development, electronics fabrication, brainstorming, equipment loan, and physical labor; the accomplishments so far would not have been possible without their help.

TABLE OF CONTENTS

page

ACKNOWLEDGMENTS 4

LIST OF TABLES 7

LIST OF FIGURES 8

LIST OF ABBREVIATIONS 10

ABSTRACT 12

CHAPTER

1 MOTIVATION 14

Problem Statement 14
Legal Implications 14
Sea Level Trends 16
Current Data and Techniques 17
Recent Literature 18

2 SEA LEVEL COMPLEXITY AND ANALYSIS 22

Tidal Forces 22
Tidal Variation 23
MHW and MSL 25
Tidal Boundaries 26
Boundary Determinations 27
Tide Study Methods 27
The height difference method 28
The amplitude ratio method 28
The range ratio method 29
Tidal Datums in Bays 29
MHWL Mapping 30
Tidal Datum Model 31
Intertidal Zone Model 32
Surface Intersection Algorithm 33
SLR Impact Prediction 34
Site Conditions 35

3 CLOSE-RANGE AERIAL REMOTE SENSING 39

Topographic Modeling 39
CARS System 39
CARS Components 41

CARS Design Considerations 43

4 TOPOGRAPHIC MODELING PILOT STUDY 45

CARS Performance Evaluation 45
GPS Evaluation 46
IMU Evaluation 51
Camera Evaluation 53
CARS Test Range Procedures 54
Coastal Testing 55
Mangrove Coastline Testing 56
Bare Earth Testing 57
Sun Angle Testing 57

5 SUMMARY AND CONCLUSIONS 70

Summary 70
Conclusions 72

APPENDIX

A ANTENNA TESTING 74

B WESTWARD BIAS INVESTIGATION 81

C BORESIGHT CALIBRATION 88

LIST OF REFERENCES 91

BIOGRAPHICAL SKETCH 95

LIST OF TABLES

Table		page
4-1	CARS GPS error statistics	59
4-2	Horizontal position errors of the antenna testing campaign	59
4-3	CARS IMU gyro drift performance	59
B-1	East and North DOP in four regions of the world	83
C-1	Boresight calibration coordinates	89

LIST OF FIGURES

Figure		page
1-1	SLR trend at Cedar Key, Florida over the last 95 years	21
1-2	Effect of 20 years of SLR on lot area with 10:1 slope	21
2-1	Effect of 20 years of SLR on example inlet area	37
2-2	Midnight Pass, Sarasota, Florida (Google Earth imagery)	37
2-3	MHWL mapping data processing flow	38
2-4	Elevation modeling site conditions	38
3-1	Components and Data Flow of CARS System	44
4-1	Control network of the CARS test range	60
4-2	Control network baselines of the CARS test range	61
4-3	CARS AC12 GPS receiver performance	61
4-4	Satellite configuration over 90 minute session using GPS patch antenna	62
4-5	Elevation angle of satellites from 90 minute patch antenna session	62
4-6	nIMU z-Gyro Noise Characteristics	63
4-7	GPS/IMU sychronization Clock noise charecteristics	63
4-8	GPS/IMU sychronization Clock jitter charecteristics	64
4-9	UAV Simulator Boom	64
4-10	Precision of the CARS GPS trajectory	65
4-11	Sample of uncorrected CARS imagery of the test range	66
4-12	CARS aerial assembly with coordinate system axes and offsets	67
4-13	Coastal study Site 1 and Site 2 (image from Google Maps)	68
4-14	Coastal study Site 3 (image from Google Maps)	68
4-15	Example of CARS imagery showing forward overlap	69
A-1	Ground planes compared during antenna testing	75

A-2 Effect of ground plane size on GPS signal reception..... 76
B-1 East and North DOP in four regions of the world..... 83
B-2 East and North DOP values over a year..... 84
C-1 Boresight calibration GCPs..... 90

LIST OF ABBREVIATIONS

1PPS	One pulse per second
AGL	Above ground level
AT	Aero-triangulation
CARS	Close-range Aerial Remote Sensing
CCD	Charge-coupled device
COM	Computer on module
CORS	Continuously operating reference station
CP	Control point
DEM	Digital elevation model
DOP	Dilution of precision
FAA	Federal Aviation Administration
FEMA	Federal Emergency Management Agency
FPS	Frames per second
GPS	Global Positioning System
GSD	Ground sample distance
IMU	Inertial measurement unit
IPCC	Intergovernmental Panel on Climate Change
LiDAR	Light detection and ranging
MEMS	Micro-electro-mechanical system
MHW	Mean high-water
MHWL	Mean high-water line
MSL	Mean sea level
NOAA	National Oceanic and Atmospheric Administration
NAD83	North American Datum of 1983

NAVD88	North American Vertical Datum of 1988
NTDE	National Tidal Datum Epoch
PDOP	Position dilution of precision
PSCP	Paint stripe corner point
RMSE	Root mean square error
SD	Secure Digital
SLR	Sea level rise
TDS	Tripod Data Systems
UAV	Unmanned aerial vehicle
USB	Universal Serial Bus
USC&GS	United States Coast and Geodetic Survey
UTC	Coordinated Universal Time
VTOL	Vertical take-off and landing

Abstract of Thesis Presented to the Graduate School
of the University of Florida in Partial Fulfillment of the
Requirements for the Degree of Master of Science

MARRYING TOPOGRAPHY AND TIDES; A HIGH RESOLUTION TIDAL DATUM AND INTERTIDAL ZONE ELEVATION MODEL FOR IMPROVED DETERMINATION OF SHORT TERM SEA LEVEL RISE IMPACTS IN FLORIDA BAYS

By

Nicholas DiGruttolo

December 2010

Chair: Ahmed Mohamed
Cochair: Grenville Barnes
Major: Forest Resources and Conservation

One of the greatest challenges coastal regions of the world face is the threat of the rising sea. Current geospatial models of coastal areas at risk of inundation by sea level rise (SLR) typically depict a 50 year timescale. The relatively long time of 50 years is due to a lack of data accurate enough to support shorter term predictions. I hypothesize that a geodetic-grade digital elevation model (DEM) of the intertidal zone overlaid onto a high resolution model of the mean high-water (MHW) tidal datum will allow for mapping the mean high-water line (MHWL) at an accuracy of less than 40 mm; this level of accuracy will allow the effects of SLR on property boundaries and infrastructure to be determined on a 20 year timescale. The need for a high resolution model of the MHW tidal datum is especially important in Florida's bays. Over 11,000 km of Florida's tidal coastline are to some extent disconnected from the open water, resulting in a need for precise tidal data to accurately determine the effects of less than 40 mm of SLR.

The study demonstrates the need for geodetic-grade elevation data and densely spaced tide level measurements for intertidal zone modeling. This level of detail is

required for mapping the MHWL and existing data do not provide the necessary detail. This work shows the potential for acquisition of elevation data to produce a high resolution intertidal zone DEM with a remote sensing system carried by an unmanned aerial vehicle (UAV).

Finally, I developed and tested a low-cost, easily deployable, Close-range Aerial Remote Sensing (CARS) system capable of obtaining geodetic-grade elevation data. I describe system design considerations and discuss preliminary results from simulation and field testing. I conclude that a low-cost CARS system weighing less than 200 grams that consumes less than 4 watts meet the requirements to map the effects of SLR on a 20 year timescale.

CHAPTER 1
MOTIVATION

Problem Statement

Predictions vary significantly as to the rate at which sea level rises. However, the evidence is strong that sea level rise (SLR) is already occurring and will continue in the future (United States 2007). Shallow slopes near the coast mean that a small vertical rise in sea level can create a large horizontal shift at the interface of the sea and the land that makes up the shore. This horizontal shift has the potential to have a major impact on littoral property boundaries and vegetation. To improve the accuracy of the mean high water line's (MHWL) location, this study set out to increase the precision and accuracy of both the mean high water (MHW) tidal datum and the elevation model of the intertidal zone above that which is typical in the practice of surveying today. This increase in horizontal accuracy of the MHWL allows for shorter term predictions of the effects of SLR on land boundaries. Specifically, this study focuses on isolated bays in Florida that demonstrate altered tidal oscillations that in turn modify the effects of SLR.

Legal Implications

The MHW tidal datum is the legal boundary between private upland ownership and public ownership of submerged lands in many states. The U.S. Supreme Court ruled in 1939 that the MHW tidal datum defined a precise and scientifically derived line equivalent to the English common law term, the ordinary high water mark, which most states used to define riparian boundaries at the time (Briscoe 1983). Based on the definition by the U.S. Coast and Geodetic Survey (USC&GS), MHW is the average of all the high waters at a place over the 18.6 year lunar cycle (Cole 1997). Therefore, land

boundaries that refer to the MHWL are ambulatory and SLR has the potential to have a major impact on the legal ownership of some of the most valuable coastal land.

The current National Tidal Datum Epoch (NTDE) published by the National Oceanic and Atmospheric Administration (NOAA) at control tide stations determines the legal elevation of MHW on which local tide studies are based. The immediate change in the MHWL when a new NTDE is adopted by NOAA at approximately 20 year intervals alters property boundaries (Gibson 2010). A dramatic shift in property boundaries can occur, in areas where seawalls were built at low elevations, due to the effect of the MHWL staying at the seawall face until SLR causes the elevation of MHW to exceed that of the top of the seawall. Once the elevation of MHW exceeds the height of the seawall, it is possible that large amounts of filled property could be transferred to public ownership. This could happen in a very short time due to the extremely flat terrain upland of many older seawalls. In response to boundary questions related to the repeal of the Butler Act, chapter 253.12(9) of the Florida Statutes grants title of land filled prior to July 1, 1975 to the riparian owner in certain instances. Although I have found no case law related to the submergence of seawalls due to SLR the courts will need to decide if current waterfront lots will be allowed to rise with fill to become islands as the surrounding area is submerged by SLR. The Mississippi Supreme Court, in *Cinque Bambini Partnership v. State*, found that SLR affects private ownership.

> If over decades, . . . the tides rise -- that is, the mean high water mark rises (and there is reason to believe this has happened and may continue to happen) -- the inward reach of the tidal influence expands…[T]he new tidelands so affected accrete to the trust (Fischman 1991).

A recent article in the *Vermont Journal of Environmental Law* states that SLR does not fit with the well established common law upon which courts historically have based tidal

boundary decisions (Sax 2010). The article states that SLR is neither gradual like accretion nor sudden like avulsion. I think it is obvious that the temporal scale is much closer to accretion than avulsion but that has not been definitively decided by the courts.

Sea Level Trends

Figure 1-1, a graph of almost continuous sea level observations for the last 95 years at Cedar Key, Florida, indicates a 1.8 mm/year rise in sea level (NOAA 2010b). SLR affects ownership of the most valuable property in Florida. Very small waterfront lots and strict land development regulations mean that a parcel of land may be rendered unbuildable by a very small reduction in its size due to SLR. For example, a 0.1 hectare (1/4 acre) waterfront lot in Florida with a 10:1 shoreline slope will experience a 36 cm landward shift in its property boundary with the 3.6 cm SLR measured over the last 20 years. If this lot had a dimension of 30 m along the shore then the property owner would have lost 10.8 m^2 (116 ft^2) of land. At an average land value of $200,000 (the least expensive comparable lot I found) the monetary impact is $2,160. This impact pales in comparison to the reduction in value that would occur if the loss of 10.8 m^2 of land made a vacant lot unbuildable due to minimum area requirements in the land development regulations. Figure 1-2 depicts this scenario.

The Intergovernmental Panel on Climate Change (IPCC) estimates SLR will “very likely” exceed the current rate of 1.8 mm/yr in the 21st century (IPCC 2008). Knowing the exact elevation of the coast and reliable estimates of SLR provide key inputs into the calculation of how much land will be inundated. A change in sea level of 1.8 mm is undetectable for all practical purposes on natural ground or even in relation to a seawall cap; however, 20 times this amount, 36 mm, is detectable with precise measurements. Based on a linear rise in sea level of 1.8 mm/yr a 20 year period is the shortest

timeframe for which realistic, cost-effective measurements can be made regarding movement of the MHWL. Although, the trend towards increasing SLR or amplification of its effects in isolated bays will allow for shorter timescale analyses as changes will reach a detectable threshold more quickly. The vast majority of currently available coastal elevation data are not accurate to 36 mm.

Current Data and Techniques

Florida, for example, has devoted $24.5 million to acquire an elevation model of the entire coastal zone with Light Detection and Ranging (LiDAR) technology (Butgereit 2009). The Florida LiDAR data, collected to exceed the Federal Emergency Management Agency (FEMA) vertical accuracy specification for flood hazard mapping of 320 mm, is accurate to 180 mm (Dicks 2006). Based on the observed SLR of 1.8 mm/yr in Florida the LiDAR data may contain errors equivalent to 100 years of SLR. Therefore, a more accurate elevation model would allow for much shorter time scale analysis of the effects of sea level rise on Florida's coastline.

"Sea level change is a product of the adjustment of both ***the land and the sea***" (Pilkey and Dixon 1996). For this reason the precise and accurate measurements of the topographic elevations and tide levels must be collected concurrently to produce a map of the MHWL accurate to 36 mm. Just as swaths of LiDAR elevation data a few kilometers wide along the coast augment a coarser DEM that covers the entire state of Florida, higher accuracy swaths of elevation data a few meters wide along the intertidal zone can augment the existing LiDAR based DEM.

In an August 2007 Report to Congressional Requestors on climate change, the U.S. Government Accountability Office states "resource managers do not have sufficient site-specific information to plan for and manage the effects of climate change on the

federal resources they manage." According to the U.S. Climate Change Science Program, Synthesis and Assessment Product (SAP) 4.1, *Coastal Sensitivity to Sea-Level Rise: A Focus on the Mid-Atlantic Region*, "existing elevation data for the mid-Atlantic United States do not provide the degree of confidence needed for local decision making" (Titus 2009).

Until recently, the accuracy of the terrain and water surface models was not considered to be as important as the "consistency" of the data (Parker 2001). The inability to compare existing DEMs with hydrographic surveys spurred NOAA to create the Vdatum application for transformation of vertical data between 26 different datums, http://vdatum.noaa.gov/. Being able to directly compare elevation data derived using modern techniques, that are likely referenced to a three-dimensional datum such as the North American Datum of 1983 (NAD83), and other data that may reference a tidal datum or an orthometric datum such as mean low-water (MLW) or the North American Vertical Datum of 1988 (NAVD88) is of great importance. Failure to consider the difference in datums can introduce over 1 m of error (NOAA 2010c). However, even with the detailed hydrodynamic models NOAA created in the areas that Vdatum was tested and precise geoid models the vertical uncertainty of a transformed elevation exceeds 8 cm (NOAA 2010a).

Recent Literature

The current and worldwide interest in SLR is demonstrated by the December 2009 publication by the journal of *Water, Air, & Soil Pollution: Focus* of an article titled "Inundation Analysis in the Coastal Area Considering Climate Change Due to Global Warming" (Pokharel et al. 2009). The article investigates the effect of SLR of 1 m on the existing sewer system in Nagoya, Japan. In the article is a reference to the IPCC

prediction of a maximum of 58 cm of SLR by the end of the century. Therefore, the 1 m effects investigated may not be realized for almost 200 years.

Other recent research involves the use of DEMs in the analysis of tides to a very accurate level. In October 2009, the journal *Estuarine, Coastal and Shelf Science* published an article titled "Exploring LiDAR data for mapping the micro-topography and tidal hydro-dynamics of mangrove systems: An example from southeast Queensland, Australia." In the paper, a 5 cm accuracy DEM and precise tidal data were used to predict the potential habitat for the aedine disease vector mosquito (Knight et al. 2008). The article notes that "the elevations that distinguish the relevant areas may be quite small, a matter of centimeters."

The January 2009 issue of *Geophysical Journal International* contains an article that illustrates how closely related SLR can be to geodesy and the movements of the solid Earth. According to the article "Trends in UK mean sea level revisited," geological uplift or subsidence of the land surface and variability in atmospheric pressure may cause as much change in the interface of the sea with the land as SLR and must be considered when predictions are made as to the amount of inundation (Woodworth et al. 2009). In many cases in the study area, the uplift and subsidence is equal in magnitude to SLR at around 1 mm/yr thereby either doubling or negating the effect of SLR. These factors were not investigated as a pert of this study.

Miniaturization and cost reduction of Global Positioning System (GPS) technology is a topic with much current interest throughout the world as well. Even with the availability of tiny GPS receivers in devices such as cellular telephones, this topic has not reached a point where it can be considered trivial. In fact, at any cost, centimeter

accuracy positioning from a complete, low-cost, GPS system under 100 gm is unavailable for purchase commercially; that is why I needed to develop a system for data collection.

Recent studies indicate that more accurate elevation models can be produced with photogrammetry than with LiDAR by acquiring imagery with extreme amounts of overlap (Wiechert and Gruber 2009); “the achievable height accuracy is better than the GSD (ground sampled distance)” when 10 cm GSD imagery is used (Wiechert and Gruber 2009).

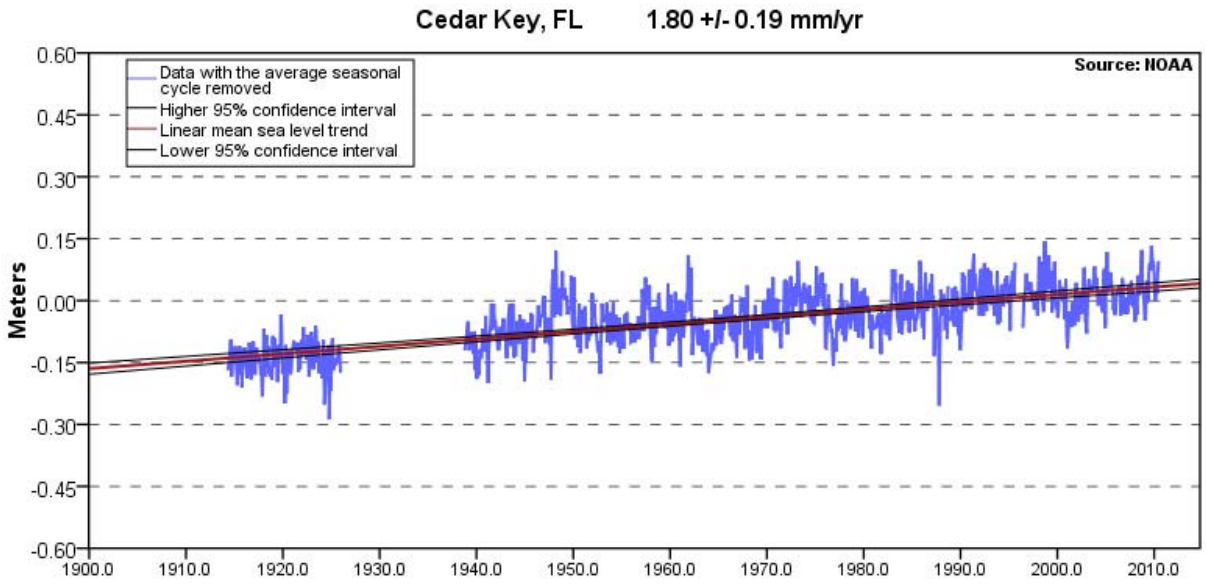

Figure 1-1. SLR trend at Cedar Key, Florida over the last 95 years

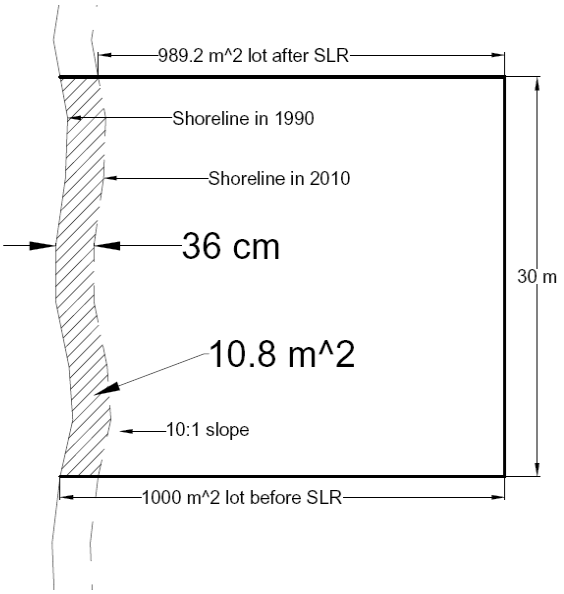

Figure 1-2. Effect of 20 years of SLR on lot area with 10:1 slope

CHAPTER 2
SEA LEVEL COMPLEXITY AND ANALYSIS

Tidal Forces

Tidal movement results from the gravitational attraction of the moon and sun acting upon the rotating earth. Horizontal tidal currents as well as the rise and fall of the water are both caused by these forces (Schurman 1941). Although mathematical formulas exist for calculating the force of gravity, tidal movement is complicated by effects of friction and inertia as the water moves over and around the landscape. In addition to the gravitational attraction of the moon there is the outward centrifugal force caused by the earth's rotation. This centrifugal force exceeds the lunar attraction at a point on the opposite side of the earth from the moon. The centrifugal force of the earth spinning on its axis combines with lunar attraction to create two tides a day in much of the world.

Applying only Newton's laws of gravitation would result in two symmetrical tidal bulges that would rise a maximum of 0.5 m above the normal sea level at the equator. These bulges would be directly below and opposite the moon's location and would travel east to west as the earth rotates (Pugh 1996). However, this theoretical tide is far from the observed tides of the earth. Movements of water on the surface of earth propagate as long waves but are impeded by the continents. Even if these waves were not impeded by the continents they would be unable to produce the full tide level given by Newton's laws of gravitation due to the depth of the water being too shallow to fulfill the hydrodynamic equations of continuity and momentum balance (Pugh 1996).

Because of the restrictions created by the continents, each ocean basin has its own tidal frequency. Most oceans have two high and two low waters each day and the

amplitude of the tide exceeds that which would be predicted with only the laws of gravitation. As the long waves created by the attraction of the moon near shallow water close to shore the change in the ratio of the wave's amplitude to the water depth causes an increase in their amplitude (Pugh 1996).

In addition to the changes to the tides caused by their long-wave properties, tides are influenced by curved horizontal currents created by the Coriolis effect. Friction on the ocean floor that slows the waves varies from place to place with the changing topography and further complicates the tide level. "Exact mathematical solutions for the complicated combinations of these factors which apply in particular shallow-water conditions are seldom possible" (Pugh 1996).

Tidal Variation

Unique characteristics that create greatly varying tides from place to place can be easily altered by human intervention such as dredging or building tidal power stations (Pugh 1996). Restriction of the free flow of water in and out of bays alters the tidal oscillations. The magnitude and direction of the difference in tide height in bays as compared to the outer coast is driven by very complex interactions of the tidal bulge with the topography of the inlet. In certain situations the shape and depth of a bay can cause extreme amplification of high tides. A well-known example of this phenomenon is the Bay of Fundy, where tidal ranges sometimes exceed 10 m (Pugh 1996). The opposite can also occur. At areas in bays that are a long distance from an inlet it is common for the tidal influence to be greatly diminished or nonexistent. The location where the tidal influence ends is called the head of tide (Cole 1997). The latter situation is of the most concern for this research. The location of the head of tide moves as sea level rises and more water flows through the inlets into the bay. Due to the head of tide

being a product of not just the height of the tide but also the duration of the rise and fall, a measurement in SLR of 10 mm at the inlet will not correspond with a 10 mm rise in MHW as the head of tide is approached. The amount of increase in MHW near the head of tide will be larger than that of SLR at the inlet due to increased flow.

It is logical that mean sea level (MSL) in a bay will rise or fall by approximately the same amount as does MSL on the outer coast, but an increase in the flow rate of water through an inlet due to SLR will likely amplify the effect on the MHW. For example, a 100 m wide inlet with 10:1 side slopes and a depth of 1 m has a cross sectional area of 110 m^2. With a 36 mm increase in depth due to SLR (20 years at 1.8 mm/yr) the cross sectional area of the inlet increases by 4% to 114.3 m^2, (Figure 2-1). A corresponding 4% increase in flow rate through the inlet would be expected, based on a 0.25 m/s tidal velocity, even more if the reduced friction impeding tidal flow through the larger inlet is considered. The product of the velocity and the cross sectional area estimates the flow rate through the inlet.

$$\frac{0.25m}{s}110m^2 = \frac{27.5m^3}{s} \text{ before SLR} \quad (2\text{-}1)$$

$$\frac{0.25m}{s}114.3m^2 = \frac{28.6m^3}{s} \text{ after 20 years of SLR} \quad (2\text{-}2)$$

For this reason, amplification of the effects of SLR in isolated bays must be considered when communities plan for the future.

According to Florida Sea Grant, there are 13,271 km of tidal coastline in Florida and only 2,173 km of general coastline (Florida Sea Grant 2010). This means that 11,098 km of tidal coastline are to some extent disconnected from the open water. It

also means that several thousand kilometers of the tidal coastline are subject to altered tidal oscillations which can magnify the effects of SLR.

MHW and MSL

MHW is calculated much differently than MSL. MHW is calculated from only high-water measurements, which occur either once or twice daily, depending on the type of tides that occur in the area. Three main types of tides exist and the characteristics of the tide at different places with the same type will be similar except for the time and range. The characteristics at places with different types of tides will differ dramatically, even if the time and range of the tides are similar. H. A. Marmer, a former Assistant Chief of the Division of Tides and Currents for the USC&GS, states that "…differences in time and range of tide are merely differences in degree, but differences in type of tide are differences in kind" (Marmer 1951).

The three types of tides are; 1. diurnal, sometimes referred to as daily, 2. semidiurnal, also referred to as semidaily, and 3. mixed, because it can change between semidiurnal and diurnal. Tides of the diurnal type complete a cycle of high and low water in one tidal day, or 24 hours and 50 minutes. Tides of the semidiurnal type complete a cycle of high and low water in half a tidal day, or 12 hours and 25 minutes. A mixed tide usually has two highs and two lows each day but one high and one low may be much different or not even noticeable on a chart of the water level at certain times.

Florida's east coast experiences semidiurnal tides with two tidal cycles each day that have approximately the same amplitude (Thompson 2000). Florida's west coast also experiences two tidal cycles each day but the amplitude of the cycles varies and

forms a mixed tide (Thompson 2000). The panhandle of Florida experiences diurnal tides, as does Tampa Bay and Charlotte Harbor (Thompson 2000).

There is an important difference between MSL and mean tide level (MTL). MSL is the arithmetic mean of all observed hourly heights spanning the National Tidal Datum Epoch. In many places the tide does not rise at the same rate at which it falls. When this difference occurs the arithmetic mean can differ significantly from the mean of the high and low waters. The mean tide level, on the other hand, is the arithmetic mean of calculated mean high water and mean low water values. Today this datum plane is rarely used except in calculations but historically it was of great importance. According to Tidal Datum Planes, a special publication of the USC&GS:

> Prior to the invention of the automatic tide gauge the recording of the tide throughout the 24 hours of the day was a matter of considerable expense. It was therefore customary to observe the tide only near the times of high and low water. This permitted a tabulation of the high and low waters but not of the hourly heights. Half tide level could be determined from such tabulations, but not mean sea level; and as a rule the early determinations were those of the plane of half-tide level (Marmer 1951).

MHW is calculated based on the observed MTL at a tide station, not MSL. Therefore, changes in property boundaries determined by MHW cannot be analyzed using trends in MSL directly.

Tidal Boundaries

"It has been reported that science finds an occasional use for tidal datums, though it may appear they are produced solely for the purposes of lawyers" (Briscoe 1983). Construction near the coast and activities such as shipping surely benefit from the determination of tidal datums to protect persons and property from harm, but one of the primary uses of tidal datums is for the determination of boundaries of land ownership. Not all states recognize the mean high water line as being the boundary of private

ownership. Some states, such as California, were territories owned by countries other than England before entry into the union and had different laws regarding the ownership of tidelands that still apply. Others, such as Massachusetts, had long-standing practices that recognized private ownership down to the low water line (Thompson 2000). Even the various courts' decisions differ in how the law is interpreted.

Boundary Determinations

No matter which datum is used in the jurisdiction in which a boundary line is being determined, a tidal datum will need to be established for the individual site of the property. Due to the difference in the datum of mean high water within a bay as compared to that of open water, even short distances may change the elevation of the mean high water line. In order to establish the true elevation of the mean high water line a tide study must be performed. For example, Chapter 177.38 of the Florida Statutes, *Standards for establishment of local tidal datums*, states "A local tidal datum must be established from a series of tide observations…" and Chapter 177.39, *Determination of mean high-water line or mean low-water line*, indicates that geodetic benchmarks shall not be used for determining the MHWL unless approved by the Department of Environmental Protection.

Tide Study Methods

The method chosen for determining a tidal datum at a specific site may vary depending on the site's location. In general, if no conditions separate the influence of the tide between a published tidal benchmark and a remote site then the tidal datum can simply be extended and considered to be equal at the bench mark and the remote site. If conditions do exist that could cause the tidal datum to differ between the

benchmark and the remote site then a method of interpolation or extrapolation must be used.

To extend tidal datums into areas not covered by primary determinations, covering an entire tidal epoch, the National Ocean Service (NOS) sets secondary and tertiary control tide stations. Secondary control tide stations have less than 19 years of continuous observations but more than 1 year. Tertiary stations have less than 1 year but more than 30 days of continuous observations (Center 2000).

To extend tidal datums into areas not covered by at least an NOS tertiary control tide station local surveyors must determine the local tidal datum by an approved method. The methods approved for use in Florida are:

- **Height Difference Method –** Observes only the high waters at the benchmark and the remote site.
- **Amplitude Ratio Method** – Observes both the high and low waters at the benchmark but only the high waters at the remote site.
- **Range Ratio Method** – Observers both the high and low waters at both the benchmark and the remote site.

The height difference method is approved for use by the Florida Department of Environmental Protection, Bureau of Survey and Mapping for use only in situations where the difference in the range of tide at the benchmark and the remote site are within 10% of each other and differential leveling from a tidal or geodetic benchmark is impractical (FDEP 2003).

The amplitude ratio method is used when the entire tidal cycle cannot be measured at the remote site. Large areas of shallow water may make it difficult to mount a tide staff in a location where low water can be observed. This method requires water levels are observed at 6-minute intervals at both the benchmark and the remote site (FDEP 2003).

The range ratio method is the most accurate method for determining tidal datums at a remote site (FDEP 2003). The range ratio method has simpler calculations than the amplitude ratio method but can only be used where observations of both high and low water can be made at the remote site.

Regression analysis has been suggested to provide a more statistically valid solution for MHW but currently the Florida Department of Environmental Protection only lists the three methods above as acceptable procedures for determining tidal datums (Cole 1997 and FDEP 2003).

Tidal Datums in Bays

Local topography influences the tides in bays more than do gravitational forces (Cole 1997). The Coriolis effect also plays a significant role in shaping tidal datums in bays. The conservation of mass principle dictates that the height of the tidal wave entering a bay will increase as the width or depth of the bay decreases (Cole 1997). At some distance from the inlet the losses due to friction will surpass the increased tide heights due to conservation of mass (Cole 1997). In the Northern Hemisphere, the Coriolis effect causes tidal currents to veer to the right. In bays, this effect causes the water level to be higher on one side of the bay than the other (Cole 1997).

The various forces that influence the tide in bays make prediction inaccurate. Therefore, direct measurement is the most reliable method to determine tidal datums in bays. The topography and hydrodynamic effects in a bay will change over time, resulting in differences in the tidal datums. Many of the direct measurements made at tertiary control tide stations, by NOS, in bays are several decades old. For example, tidal station 8725985 (Siesta Key, Little Sarasota Bay), was observed for one month in 1977 according to the data sheet published by NOS. The location of the tidal

benchmarks related to this station is in close proximity to Midnight Pass, which was closed to protect private property in 1983 (Morrill 1990). Obviously, measurements made when the pass was open do not accurately represent the conditions after its closure.

Figure 2-2 illustrates the current conditions at the former location of Midnight Pass which connected Little Sarasota Bay and the Gulf of Mexico. This location is a good example of the conditions that are currently lacking in SLR analysis. According to the FDEP, Land Boundary Information System (LABINS) http://data.labins.org/2003/, the difference in the tidal range between the bay and the outer coast at the historic location of Midnight Pass is 30 cm. Big Pass, located seven miles North of Midnight Pass is now one of the primary sources of tidal flow into Little Sarasota Bay. Big Pass is very similar in size and shape to the example inlet depicted in Figure 2-1. If a 4 % increase in tidal flow rate were to occur through Big Pass due to SLR, as depicted in the example, an increase in the tidal range at Midnight Pass would be expected. If the 30 cm tidal range increased by only 1% (3 mm) the effect would be equivalent to an additional 8% (3 mm/ 36 mm) SLR at Midnight Pass in 20 years.

MHWL Mapping

As shown in Figure 3-1, my proposed study method requires two streams of data to map the MHWL, namely the terrain data and the tidal data. An array of tide gauges is needed to model the surface of the MHW tidal datum. Tide gauges range in complexity from a simple staff with division marks that are read manually by an observer, to fully automated devices with telemetry to transmit data from a remote location with 2 mm typical precision (Solinst 2010). The automated instruments can be used to easily acquire tidal data for durations that were previously only observed by government

agencies at widely distributed sites and can cost under $1000. An array of automated gauges collecting 30 days tidal data is the recommended method for fulfilling this study's objective in the future.

The terrain data for this study are provided by a Close-range Aerial Remote Sensing (CARS) system with georeferencing by GPS. In Chapter 4 of this work, I show achievable precision of better than 25 mm in GPS elevation with CARS. By acquiring imagery with 80% overlap, the high level of redundancy within the photogrammetric process will reduce the elevation error below that obtained with an individual GPS position. The combined error of both data streams should be under 36 mm and split by 1/3 (12 mm) in the MHW model and 2/3 (24 mm) in the intertidal zone elevation model; this allows for the 20 year timescale delineation of SLR.

Tidal Datum Model

The first step in the production of a high precision tidal datum is simultaneous observation of water levels at a control tide station and at a sufficient number of subordinate tide stations (Marmer 1951). On the outer coast, where tidal flow is not disturbed by passage through inlets, interpolation between existing tide gauges can be performed to calculate the value of MHW within a few millimeters in many locations. In bays where no continuous-recording tide gauges are present and the head of tide has not been established recently, interpolation is not an option. Tide observations must be of a sufficient length to eliminate the effects of local conditions such as wind and stormwater runoff.

The second step of the process is to connect the subordinate tide stations and, thus, the MHW tidal datum, to the intertidal zone model. Photo-identifiable targets referenced to the tide gauges in three dimensions provide stable points to connect the

intertidal zone model derived by photogrammetric techniques to MHW. The relative orientation between the tidal datum and the topography will be determined completely within the photogrammetric process due to the visibility of the tide gauge reference points in the imagery. Therefore, the error budget of the production process, which must not exceed 36 mm to accomplish the intended goal, will not be affected by inaccuracies in the local NAVD88 network or any geoid model. When tidal and topographic data collected at different times are compared with an application such as Vdatum errors in the transformation exceed 36 mm.

Intertidal Zone Model

Conventional survey techniques for determining elevations of the intertidal zone with automatic levels or theodolites are currently the most accurate method; typically under 30 mm of error at the measured points. This method usually relies on transects collected at even intervals and additional detail collected for areas with greater relief. This method works well on open beaches; however, in bays and marshes this labor intensive data collection method is slow and expensive. In remote areas a few hundred meters of coastline may take an entire day of data collection. Low-altitude LiDAR may approach the 30 mm accuracy of conventional survey techniques and will provide virtually continuous coverage of an area with elevation data. However, currently, it requires mobilization of a helicopter that costs several thousand dollars to bring to the jobsite which makes the collection of small, frequent datasets more expensive than conventional survey techniques.

A UAV equipped with a remote sensing system capable of acquiring geodetic-grade elevation data can make mapping of the MHWL at the scale of a single municipality less expensive than LiDAR and faster than conventional surveying. The

UAV acquires stereo aerial imagery for production of a DEM by autocorrelation. Natural color imagery with a ground sampled resolution approaching 5 mm is a byproduct of the production process. Once the DEM is created the imagery is no longer necessary for mapping the MHWL but there are many other uses for imagery with 5 mm resolution. Due to Federal Aviation Administration (FAA) restrictions on flying UAVs, this research simulated the data acquisition process.

Surface Intersection Algorithm

The intertidal zone elevation model and the MHW tidal datum model will be merged to determine the MHWL. A digital image processing algorithm will be used to determine the pixels at which the intersection of the two surfaces occurs; a simple surface intersection algorithm similar to the one described in Quandros and Collier (2008) will be used for that purpose. The mathematical model for the surface intersection algorithm is as follows

$$\begin{aligned} &(IZDEM_{Pixel(n)} - MHWDEM_{Pixel(n)}) = 0 \\ &\frac{yes: MHWL_{Pixel(n)} = true}{no: MHWL_{Pixel(n)} = false} \end{aligned} \tag{2-3}$$

Where
$IZDEM_{Pixel(n)}$ is the n^{th} pixel in the intertidal zone DEM
$MHWDEM_{Pixel(n)}$ is the n^{th} pixel in the MHW tidal datum DEM
$MHWL_{Pixel(n)}$ is the n^{th} pixel in the raster image of the MHWL
If the values in the equation equal 0 (yes) then the pixel lies on the MHWL (true)
If the values do not equal 0 (no) then the pixel does not lie on the MHWL (false)

The horizontal accuracy of the final MHWL vector graphic is the top priority of this study. The horizontal and vertical errors internal to the tidal datum determination, imaging sensor positioning and the photogrammetric processes, which constitute the majority of the steps depicted in Figure 2-3, will propagate into the horizontal accuracy

of the MHWL. Since none of the processes for determining the MHWL involve an absolute vertical datum, the desired horizontal accuracy of the MHWL vector graphic will not be affected by errors in the local NAVD88 network. Connection to NAVD88 is not needed to allow overlaying of the two-dimensional MHWL onto existing maps. Given the facts that GPS is typically twice as accurate horizontally as it is vertically and that shallow slopes occur on the coast of Florida, this is of major importance. As seen in Figure 1-2, a 10:1 slope will cause ten-fold increase in the horizontal movement of the MHWL compared to the vertical change in sea level. For this reason, reduction of vertical errors in the process allows for shorter term determination of SLR effects.

SLR Impact Prediction

Once the baseline terrain and tidal data have been acquired, it will be possible to simulate scenarios of SLR. In the simplest form of analysis, the intertidal zone model will be assumed to remain constant and the tidal datum model will be elevated uniformly across the entire area of interest. By simply increasing the values for each pixel of the MHW datum raster by the amount of SLR to be investigated and rerunning the surface intersection algorithm, the horizontal impact of SLR will be depicted. More advanced prediction scenarios will be possible where historic topographic data exist at sufficient accuracy to project erosion and accretion. Multiple tidal datasets separated in time would also allow for much more detailed analysis but will not likely be available.

Additional tidal datum determinations and imagery acquisition in the future will allow projections of both SLR and topographic changes. Two datasets collected as described above and separated in time will allow for projection of the surface models into the future. With this additional information, nonlinear trends in the movement of the MHWL can also be predicted.

Site Conditions

The feasibility of determining a bare earth elevation model varies depending on site conditions. Typical conditions along the coast of Florida's bays include mangrove forests, salt marshes, and urban areas with manmade features, such as seawalls. See Figure 2-4 for examples of these conditions.

Mangrove forests typically consist of very dense vegetation that is not easily penetrated by LiDAR pulses; inaccurate results are common when LiDAR is used to produce an elevation model in this type of ground cover (FEMA 2003). Photogrammetric techniques are also hampered by dense vegetation due to the need for the same point on the ground to be visible in multiple images for elevation determination. For these reasons, imaging of some vegetated areas is best conducted at low tide to improve the acquisition of elevation data on the seaward side of vegetation; in these cases interpolation between upland and seaward data points can be performed to calculate approximate ground elevations within the vegetated area. The flexibility of the CARS system will make it much easier and more economical to acquire tide synchronized imagery than with a conventional aircraft.

Salt marshes would also benefit from imagery acquisition that coincides with low tide; this ensures that the area above the MHWL is modeled accurately by allowing standing water to dissipate to the greatest extent possible. Standing water impedes conventional LiDAR and imagery equally but acquisition of tide synchronized imagery will ensure accurate mapping of the current MHWL.

Urban areas with seawalls need not be imaged at low tide. Furthermore, until the seawall is topped by the tide, the MHWL will remain the same. Extreme tides may cause the seawall to be topped at the time of imagery acquisition; this situation must be

avoided. The majority of high tides will not cause this effect so the time of acquisition can be greatly expanded in most urban areas.

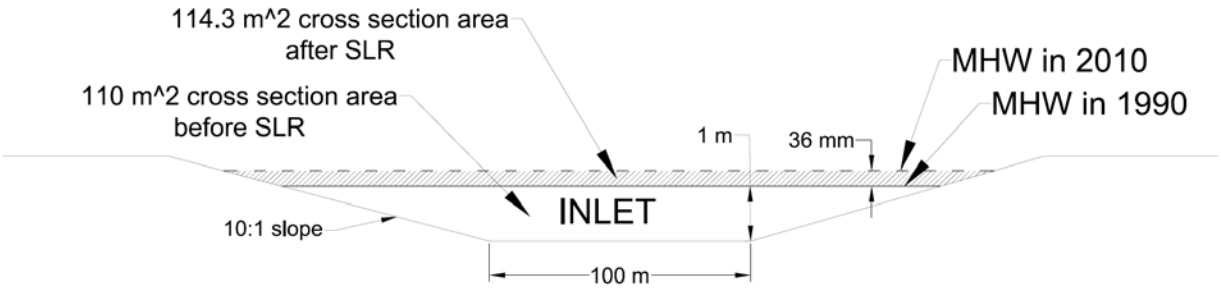

Figure 2-1. Effect of 20 years of SLR on example inlet area

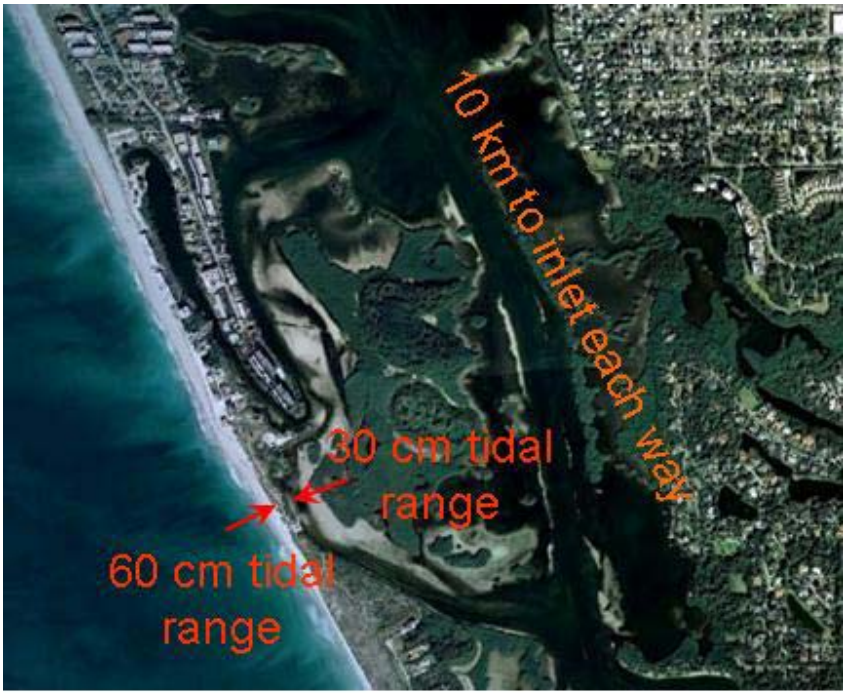

Figure 2-2. Midnight Pass, Sarasota, Florida (Google Earth imagery)

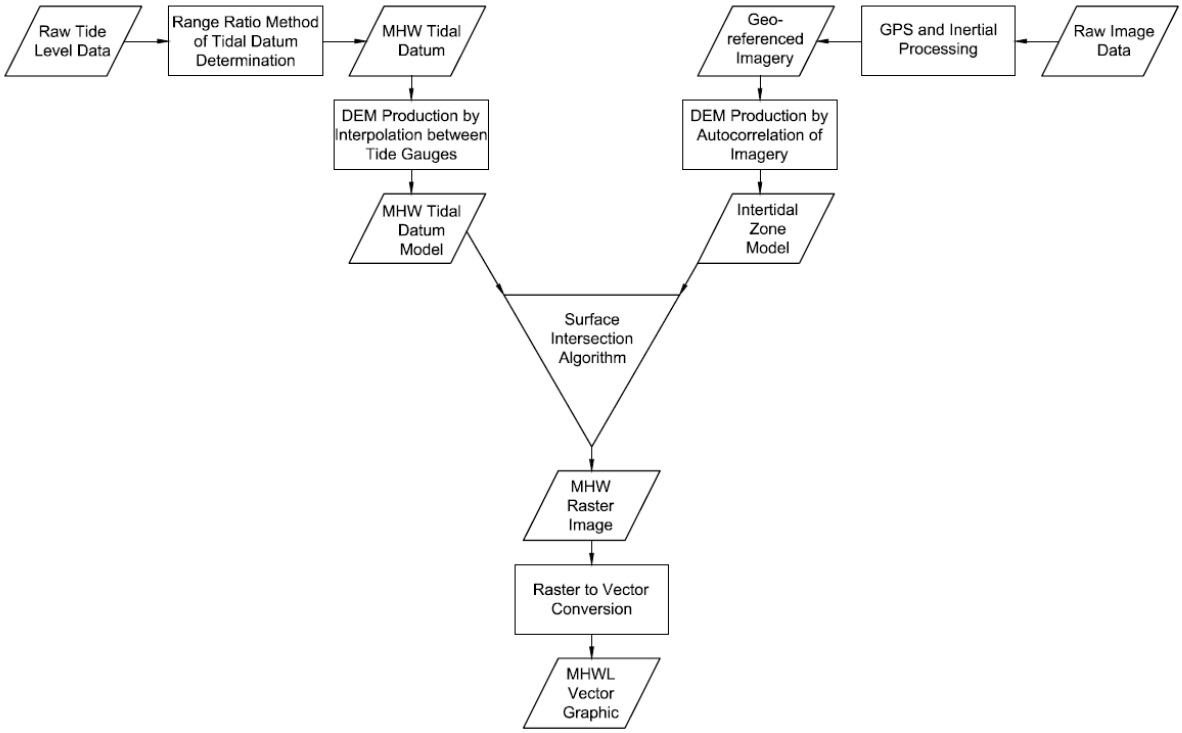

Figure 2-3. MHWL mapping data processing flow

Figure 2-4. Elevation modeling site conditions (public domain images from NOAA)

CHAPTER 3
CLOSE-RANGE AERIAL REMOTE SENSING

Topographic Modeling

Close-range, unmanned aerial vehicles (UAVs) capable of collecting remote sensing data are emerging as a new method for collecting high resolution data over specific areas. A focus of this research is on obtaining geodetic-grade georeferencing accuracy from low-cost L1 carrier phase global positioning receivers and micro-electro-mechanical system (MEMS) inertial measurement units (IMU). High accuracy georeferencing enables the production of precise orthophotos and stereo models used in the generation of the DEMs accurate to 36 mm necessary for mapping short-term effects of SLR.

Research is currently being conducted in Germany to model the flight patterns of albatross as they cross the ocean that began with the development of a “stand-alone miniaturized L1 GPS data logger” (Traugott et al. 2009). The logger is capable of collecting 5.3 days of carrier phase data at 10 Hz and weighs 25.5 gm (Traugott et al. 2009). This device, however, does not obtain the positional accuracy necessary to construct a DEM accurate to 36 mm without ground control. Similar inexpensive, L1 GPS receivers are capable of sub-centimeter kinematic positioning. Research by the Geospatial Research Center (NZ) Ltd. indicated that integer ambiguity can be successfully resolved when modified algorithms are used in processing but the success rate was less than 32% (Pinchin et al. 2008).

CARS System

The Close-range Aerial Remote Sensing (CARS) system is designed to produce an elevation model of the intertidal zone sufficient to map the MHWL on the ground with

accuracy comparable to SLR on a 20 year timescale. By integrating a 20 gm MEMS IMU to a GPS data logger similar to those described earlier, centimeter accuracy positions can be obtained when nearby reference stations are available. Waeigli and Skaloud (2009) discuss such an integration and methods for initial orientation. The Geospatial Research Center testing that resulted in a 32% ambiguity resolution rate, mentioned above, was conducted on a ground based vehicle in a high-multipath environment; the UAV platform I employ reduces the error sources that hindered ambiguity resolution. Static initialization at the beginning and end of each flight can provide sufficient data for integer ambiguity resolution and positional accuracy within a few millimeters.

Wiechert and Gruber (2009) concluded that "the achievable height accuracy (of a DEM produced from aerial imagery) is better than the GSD (ground sample distance)." If this statement holds true for 10 mm GSD imagery obtained by the CARS system, then a 10 mm accuracy DEM could be obtained along the coast of Florida for under $100 per kilometer and with a fast turn-around time. This cost estimate is based on 30 km/day of data acquisition by a single technician and automated photogrammetric processing.

The CARS system is proposed to supplement LiDAR derived terrain data with a few-meter-wide strip DEM of only the intertidal zone. Many commercially available UAVs exist at greatly varying specifications. Fixed wing UAVs typically are capable of flying faster and longer than Vertical-Take-Off-and-Landing (VTOL) aircraft; however, the maneuverability of VTOL aircraft is well suited for the task of mapping the intertidal zone. This research is developing a universal payload for multiple applications; one candidate vehicle is the Microdrones GmbH, md4-1000. The md4-1000 is a quad-rotor

VTOL UAV capable of carrying an 800 gm payload for a 70 minute flight time (Microdrones 2010).

CARS Components

Figure 3-1 depicts the flow of data between components in the CARS system. The system consists of a low-cost GPS receiver and antenna, a MEMS-based IMU, a low-cost digital imaging sensor, a central processing unit, an integration circuit board with data storage capability, and an onboard power supply. The CARS system acquires georeferenced stereo imagery that is used to produce a DEM of the intertidal zone by photogrammetric techniques.

In order to achieve the inexpensive, geodetic-grade goal of this research, two GPS receivers were considered as positioning sensors, the u-blox LEA-5T and the Magellan AC12. The LEA-5T is primarily designed for precision timing applications but it also logs carrier phase raw measurements. Much literature has been published touting the excellent results the discontinued u-blox LEA-4T can produce in kinematic positioning (for example, see Schleppe 2006). Likewise, the Magellan AC12 receiver has been the subject of multiple experiments to evaluate its potential (Alkan 2009). The AC12 has been shown to produce static positions accurate to under 3 cm on a 50 km baseline with less than 30 minutes observation (Alkan 2009). This single-frequency OEM board outputs carrier phase data and a 1 pulse per second (1PPS) signal accurate to 250 nanoseconds (Magellan 2007). The board weighs 45.4 gm and consumes 230 mW of power. The manufacturer's specifications state this receiver is capable of 3 cm accuracy (Magellan 2007). We also tested several GPS antennae, one of which is the u-blox ANN-MS-0 active dielectric patch antenna that is less than 40 mm square and weighs less than 100 gm with the magnetic base removed (U-blox 2010).

The IMU used is a Memsense NA05-0300F050C Nano Inertial Measurement Unit (nIMU). The IMU provides 3D acceleration and orientation data with a 50 Hz bandwidth in a small device that weighs only 20 gm (Memsense 2008).

The imaging sensor used is a Chameleon digital camera manufactured by Point Grey Research Inc. The Chameleon is capable of collecting 1.2 megapixel color and panchromatic images at 7.5 and 15 frames per second respectively. It is less than 44 mm square and weighs 37 gm, which makes the Chameleon an ideal compromise between payload weight and image quality for our purpose. A Sony progressive scan interline transfer ICX445 1/3" EXview HAD CCD image sensor collects data through a standard CS mount lens (Point Grey 2010). A 45 gm and 30 mm x 30$^{\phi}$ mm size Fujinon CCTV C-mount lens manufactured by Fujifilm is used with an adapter; focal lengths of available lenses range from 6 to 75 mm (Fuji Film 2010).

Onboard the completed CARS system, payload operations will be handled by an e-con Systems, eSOM270 computer on module (COM), running Windows CE 6.0 R2. The eSOM270 contains a Marvell PXA270 processor that runs at 520 MHz; the eSOM270 is the size of a standard laptop computer memory card and weighs 10 gm (E-con 2005). Interaction between the COM and the other system components is routed thru an e-con Systems Regulus carrier board. The carrier board is 114 mm x 65 mm and weighs approximately 30 gm (E-con 2005). A Secure Digital (SD) memory card is used for onboard storage of raw GPS and IMU data and raw imagery. The overall weight of the CARS system, excluding power supply, is under 200 gm (~ 7 oz) and the overall power consumption is under 4 watts. The CARS system is intended to be light weight and small in size for versatility.

CARS Design Considerations

There is minimal research focused on harnessing the geodetic-grade accuracy of lightweight GPS receivers onboard UAVs. Therefore, the development of the CARS system required a great deal of experimentation and fabricating. Immediate miniaturization of payload components is not economical if they have not been proven to deliver the required performance. Furthermore, proving the performance of a UAV payload can be difficult when off-the-shelf components are used. Simulation needs to be performed in a ground based environment to analyze each component of a remote sensing system individually and as subsystems before miniaturization and final integration. Combining all the electronic devices of the remote sensing system into a compact, lightweight assembly requires customized circuit boards and connectors along with software development for communication between devices that do not have a common native operating environment. For example, many inexpensive GPS receivers use a low-speed communication standard whereas high data rate devices require faster communication. The configuration described above entails RS-232 communication for the GPS receiver, I2C for the IMU, USB 2.0 for the camera, and SD/MMC for data storage. Each of these standards also uses different voltages that need to be addressed to avoid damage to the hardware.

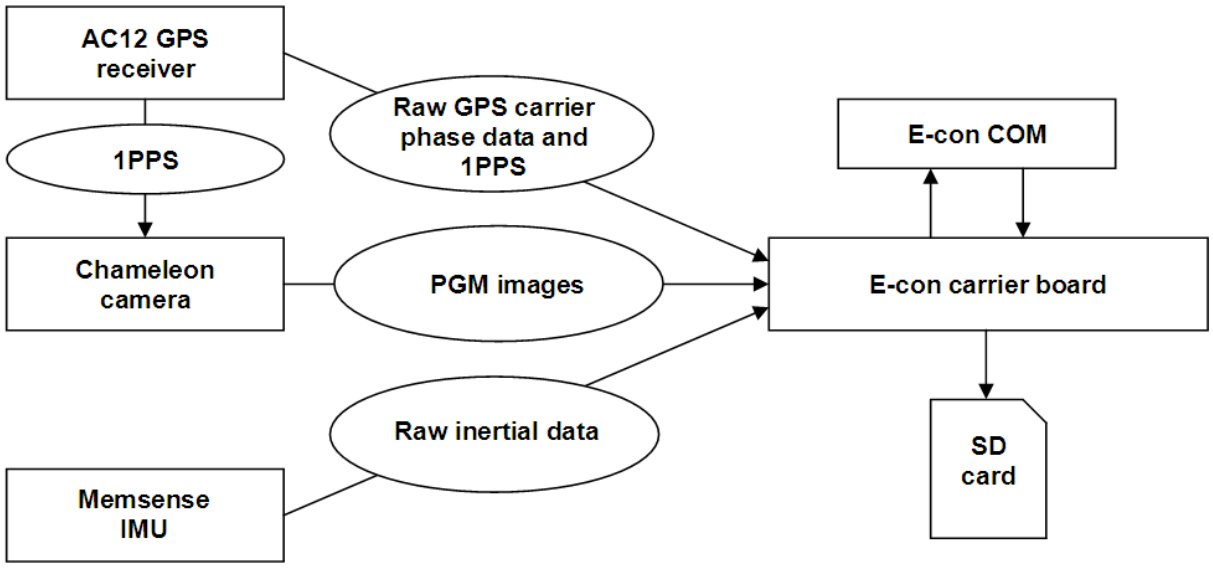

Figure 3-1. Components and Data Flow of CARS System

CHAPTER 4
TOPOGRAPHIC MODELING PILOT STUDY

CARS Performance Evaluation

A test range was established to evaluate the potential of the CARS system for topographic modeling (Figure 4-1). The test range is located on an asphalt parking lot with five rows of parking spaces delineated with paint stripes. Most of the area is free of overhead obstructions which makes it well suited for GPS observations and usable for accuracy assessment of other CARS system components. Paint stripes form a fairly consistent pattern throughout the area and are visible in existing aerial imagery. In general, the site is gently sloping with drainage swales and curbing providing some vertical relief.

To facilitate the GPS survey, a control network was established on site. The control network consists of four control points (CP) set near the corners of the survey boundary. An accurate survey of all corners of each end and intersection of every paint stripe was done with survey-grade GPS. These three dimensional coordinates were determined to be sufficiently accurate to be considered the true value for the proposed experiment if the baseline length was kept to a minimal distance, e.g., <1 cm accuracy at a 100 m baseline.

Establishing highly accurate horizontal and vertical control on the test range referenced to a geodetic datum was accomplished by simultaneous GPS observations on the control points for over five hours. Figure 4-2 depicts the network configuration. Baselines from the local continuously operating reference stations (CORS) GNVL and RLAB to CP3 and from CP3 to each of the other CPs in the network were processed using the first two hours of the five-hour observation session. The last two hours of the

session was used to process the additional independent baselines needed to create the network.

Precise relative elevations were established on the CPs by differential leveling with the CPs in a closed loop to ensure against blunders. Loop closure was calculated as 2 mm and the error was distributed amongst the control points.

In addition to establishing the CPs, the first survey campaign was used to collect the test range survey points. On the first visit, kinematic stop-and-go GPS survey methods were determined to be the most accurate method of data collection suitable for the task based on the availability of equipment and time. The equipment utilized for collection of the paint stripe corner points (PSCP) was a Leica GX1230 GPS receiver and a Leica AX1202 antenna mounted on a fixed-height pole. The receiver was run in a kinematic stop-and-go configuration with a five second pause at each discrete point.

GPS Evaluation

To make best use of the site visit and data collection effort, an additional GPS receiver was mounted to the GPS antenna pole with the Leica receiver and the Leica antenna was shared through a splitter to provide simultaneous observations with both receivers. This eliminated the need for an independent site visit to collect data with the GPS receiver being evaluated. A u-blox LEA-5T receiver was used to compare the low-cost receiver with a geodetic-grade one. The LEA-5T is one of the least expensive GPS receivers available that will output carrier phase data and an evaluation kit costs about $300.

Raw data from the u-blox receiver was recorded on a TDS Nomad data collector using the Windows Mobile software provided with the u-blox evaluation kit. The u-blox software allows for input of event markers but the workflow was determined to be too

cumbersome for efficient collection of a large number of points so discrete points were determined by matching epochs with the Leica data in post mission.

In the interest of increasing the speed of the collection and the number of points collected, a bipod was not used to stabilize the antenna pole during the five-second static sessions. It is estimated that a variation of 2-3 cm occurred in the horizontal position of the antenna over the PSCP based on observation of the movement by a second person. This 2-3 cm variation between epochs is mitigated by the averaging of five epochs of data at each point and the horizontal movement will not degrade the vertical accuracy. A total of 686 PSCPs were collected.

Post-processing was performed with NovAtel's Waypoint GrafNav version 8.10. GrafNav successfully resolved the ambiguities of the Leica data and provided accurate coordinates to be held as the true values for the PSCPs. Integer ambiguities could not be resolved for the u-box data and the float solution contains a severe westward bias in excess of 1 m. This bias is inconsistent with previous research conducted with u-blox LEA-4T receivers but the literature review did not reveal any experiments conducted with the LEA-5T for comparison. It was determined that an alternative receiver needed to be evaluated.

On the second visit to the test range the equipment utilized for collection of the PSCPs was again a Leica GX1230 GPS receiver and a Leica AX1202 antenna along with a Magellan AC12 receiver to compare possible alternatives to the u-blox LEA-5T. Again, the additional GPS receiver was mounted to the pole with the Leica receiver and the Leica antenna was shared to provide simultaneous observations with both receivers. The AC12 receiver was also chosen for its ability to output carrier phase data

for recording to an external storage device. The AC12 receiver costs less than the u-blox receiver at a cost of about $150 without a development kit. Raw data from the AC12 receiver was recorded on a TDS Nomad data collector using a custom hyper-terminal serial data collection application written for Windows Mobile 6. The custom software did not allow for the input of event markers so discrete points were determined by matching epochs with the Leica data in post mission, as was the case in the first survey campaign.

The data collection method was identical to the first survey campaign except for the point numbering and the few PSCPs that were not located to ensure against a loss of lock on any satellites. These points were typically near medians that contained shrubs and adjacent to light poles. Due to windy conditions during the second site visit, larger centering errors of approximately 4-5 cm are estimated to have occurred by visual observation of the antenna pole's movement by a second person during the data collection process. This horizontal movement will induce less than 1 mm error on the elevation at these locations.

Post-processing was again performed with GrafNav. Integer ambiguities could not be resolved for the AC12 data and initially the float solution was inaccurate. Investigation of the AC12 raw data revealed that the Doppler observation had the wrong sign; subsequent processing of the corrected raw measurements delivered excellent results. Except for a few outliers, these results, illustrated in Figure 4-3, confirm that the AC12 receiver is capable of achieving cm-level positional accuracy with a root-mean-square-error (RMSE) of about 10 mm in each horizontal direction and 20 mm in height. Table 4-1 lists the error statistics.

With acceptable results obtained from the AC12 receiver, the focus was shifted to the antenna. The ability to use a small patch antenna on the CARS system will be very beneficial in both cost and weight savings. A visit was made to the test range in order to evaluate the accuracy that can be achieved in kinematic applications when using this antenna design. Again the AC12 and Leica receivers shared an antenna through a splitter but this time a u-blox ANN-MS-0 active dielectric patch antenna was used.

This test was conducted with the same configuration as the test when good results were obtained with the AC12 receiver, with the only exceptions being the use of a patch antenna in place of a geodetic-grade unit; only 75 of the PSCPs were surveyed on this visit. My post processing results were very poor. Apparent multipath issues caused positional errors at the meter level. The patch antenna was determined to be unusable without modification.

The failure of the AC12 to collect quality data with a patch antenna in the field prompted additional testing of antenna types in the lab to determine the best one for geodetic-grade, kinematic positioning on a UAV platform. Test procedures entailed collection of datasets with the AC12 receiver with different antenna configurations but identical satellite configurations and similar atmospheric conditions. To accomplish this scenario, 24 hour datasets were collected on consecutive days. Each day, a different antenna was mounted on the same pillar at the southwest corner of the roof of Reed Lab at the University of Florida in Gainesville. The position on the lab roof, three stories above ground level, provides an unobstructed view of the sky and a CORS receiver's antenna occupies the southeast corner of the rooftop, providing an excellent source of data for post-processing.

Antennas chosen for the test included a Trimble L1/L2 Micro-centered, geodetic-grade, model 33429 with ground plane; a Trimble L1 Small Dome, mapping-grade, model 16741; and the u-blox ANN-MS, consumer-grade, model 0-005-0 used in the last field campaign. Each antenna was connected to the AC12 receiver mounted inside the building for ease of providing power and data storage capacity on a desktop computer.

A second series of antenna testing was conducted using only the u-blox antenna and the variable was the presence and/or size of a ground plane. Ground planes were constructed of 22 gauge galvanized steel sheet backed by a piece of hardboard. A 30 cm and 15 cm diameter ground plane were constructed for the second test and an 11 cm and 8 cm ground plane were constructed for the third test. A dataset was also collected without a ground plane for comparison. Each dataset contained over 24 hours of data to allow for greater choice of processing intervals.

The CORS GNVL, located at the Gainesville Regional Airport, 8 km northeast of Reed Lab, was used as the reference station for post-processing. This baseline length allowed for a realistic estimate of the obtainable accuracy of the receiver/antenna combination. The static processing was performed with Leica Geo Office 4.0 over several different durations ranging from 90 minutes down to 15 minutes for each session. All datasets were processed using the same time windows, which were selected around the period of best PDOP based on Waypoint's Toolbox 1.00 mission planning software.

The results were inconsistent in that the solution for 90 minutes of data using the geodetic-grade antenna with a ground plane differed by less than 1 mm from the results for 15 minutes of data using the patch antenna with no ground plane; both solutions

have fixed integer ambiguities. However, Geo Office provided a float solution with almost 1 meter of error for the 90 minute session from the patch antenna. It appears that the u-blox antenna experienced severe fluctuation between tracking and loss of lock on several satellites at low elevations, resulting in a dataset that Geo Office was unable to process. The DOP values and satellite elevations are plotted in Figure 4-4 and Figure 4-5 respectively. Both figures show sever fluctuation of the satellite tracking that coincides with low satellite elevations during the last two thirds of the test. Since the processing filter reports results at the end of the static session, sessions at the beginning of the three-hour periods were much better than those towards the end, especially in the case of the patch antenna. This shows the importance of mission planning for the CARS missions especially because of the inexpensive and light-weight patch antenna used.

Except for the unexpected bad results of the second test, (marked in red) with the 30 cm ground plane, and the exceptionally good results of the third test with no ground plane, the conclusion we drew from the antenna testing results in Table 4-2 is to either have a mapping-grade antenna or to include a 11 cm (4") or larger ground plane with the patch antenna. Tests 2 and 3 suggest that having no ground plane or one smaller than 11 cm in diameter is not helpful in resolving the ambiguity to its fixed integer value or achieving a consistent, stable float solution.

IMU Evaluation

The IMU used in the CARS system is a MEMSense MEMS nano IMU. The gyro drift is characterized in the manufacturer's specification sheet as +/- 1 deg/s with a maximum standard deviation of 0.95 deg/s; typical value of the standard deviation is 0.56 deg/s (Memsense 2010). Initial static data collected in the lab proves this is the

case, with measured values for the x, y and z gyros shown in Table 4-3 below. Figure 4-6 shows data collected from the z-channel gyro. Despite the high noise level and the high drift rate bias of the nIMU, it was shown in (Benjamin et al. 2010) that attitude and heading of 1 mrad (~ 0.06°) is achievable with this IMU through using geometric constraints and precise exterior orientation positions.

The IMU records are time-stamped with the GPS time through the computer clock. Because Windows is not a real-time operating system, it has limitations with time-stamping of the IMU records. GPS time is precise to about 40 nanoseconds (ns), and, although it is not reset to the solar time, it is synchronized with UTC time to within 1 micro-second (us) (Alan et al. 1997). Figure 4-7 shows the computer clock noise between the GPS pulses every second. The graph shows a dominant computer clock bias of about 30 micro-seconds. The dominant error, nevertheless, follows the normal distribution leading us to conclude the computer clock is trustworthy for timekeeping in our application (DiGruttolo and Mohamed 2010).

The IMU's logging rate is nominally 150Hz with a nominal cycle duration of 6.67 milli-seconds (ms). Figure 4-8 shows the cycle duration between records where it exhibits a 1 ms jitter every 6 and 7 ms and a quasi-periodic delay of an additional 7-11 ms (DiGruttolo and Mohamed 2010). This behavior is due to the operating system and hardware, as slightly different results are obtained using different platforms. The clock jitter and noise produce an overall root-mean-square time error of about 200 us (DiGruttolo and Mohamed 2010). Due to the misbehavior of the Windows XP operating system, although not a limiting factor, we decided to use Windows CE, a real-time operating system.

Camera Evaluation

Progress on the interface and timing synchronization between the camera and GPS receiver allowed for independent field testing of a subsystem of the CARS. Without the inclusion of a microprocessor in the subsystem, a laptop computer was used to run the applications and for data storage. In order to simulate the motion of a VTOL UAV inexpensively, a dedicated device was fabricated. A UAV Simulator Boom was constructed for the acquisition of near vertical imagery from an altitude of 6 m above ground level (AGL). Figure 4-9 depicts the fabricated simulator boom.

The UAV simulator boom was used to collect GPS data and vertical imagery of the PSCPs for evaluation before miniaturization of system components. The configuration of the equipment entailed a rigid mount aligning the GPS antenna with the camera axis raised by the boom to altitude and the GPS receiver and laptop computer at ground level. Triggering of the camera was performed by the 1PPS signal from the GPS receiver and a custom application, CapturePGR, recorded the computer system time and image file name. Another custom application, CaptureAC12, recorded GPS time and computer system time for post-mission synchronization. A 12.5 mm focal length lens provided ground coverage (GC) in the forward direction and the transverse direction of 1.7 m and 2.3 m respectively on the 3.6 mm x 4.8 mm (1/3”) CCD for a ground sample distance (GSD) of 1.8 mm based on the formula for a vertical photograph (Wolf and Dewitt 2000).

$$GC = a\frac{H}{f} \tag{4-1}$$

Where
H is the flying height AGL in meters

f is the lens focal length in meters
a is the CCD length or width in meters

The Chameleon is capable of taking 15 frames per second (FPS) at full resolution. The critical velocity of the vehicle in Km/h would then be 6X the flying height above ground in meters; e.g. at a flying height above ground of 6 meters, 80% forward overlap between imagery is achievable at a vehicle speed of 36 km/h (~ 20 mph).

CARS Test Range Procedures

The vehicle mounted UAV Simulator Boom was raised and a 10 minute static initialization period was observed before the vehicle was set in motion. Once the image capture application was started, the vehicle was driven forward slowly to ensure that overlap in the images was sufficient for stereo coverage at the 1 FPS rate collected for this test. A subset of the PSCPs was imaged with each transit of the test range. Four transits were made, one with the Trimble mapping-grade antenna, one with the patch antenna and no ground plane, and two with the patch antenna and the 30 mm ground plane. At the end of each transit, a five minute static period was recorded by the GPS to aid reverse processing of the kinematic data.

Figure 4-9 shows results of processing the GPS raw data. As expected, the Trimble antenna performed best and the patch antenna without ground plane performed worst. In the two runs of the patch antenna using the ground plane, the positional accuracy was within 5 cm. Figure 4-10b, the graph of data collected with the patch antenna and a 30 mm ground plane, shows positional accuracy worse than Figure 4-10d, another graph of data collected with the patch antenna and a 30 mm ground plane, due to the lack of a sufficient static initialization of the system.

Figure 4-11 shows imagery taken by the CARS camera at the test range. The quality and resolution of the imagery is sufficient for the SLR application. The simulation studies show that with tight georeferencing obtained by the CARS GPS/IMU sub-system, and by carefully processing the stereo models, cm-level elevation accuracy is obtainable.

Coastal Testing

A fully functional version of the CARS system was deployed into a real-world environment to determine the suitability of the imagery for creation of the intertidal zone DEM. Figure 4-12 shows the configuration of the aerial component of the CARS system as it was used for these tests. Three coastal sites in Nokomis, Florida were chosen for their representation of typical site conditions and vehicle access within range of the UAV Simulator Boom. With a 6 mm focal length lens on the camera the GC increased to 4.9 m perpendicular to the direction of travel and the GSD increased to 3.8 mm. The 4.9 m swath width of the imagery required vehicle access within 2.5 m of the water's edge at low tide. This condition is difficult to find in coastal areas of Florida today and required an extensive search.

Sarasota County was selected for the search for a suitable site due to my personal knowledge of the area. Google Earth and Google Street View were then used to create a list of candidate sites for further reconnaissance. The Town of Nokomis was determined to provide the most diverse shoreline conditions that met the access requirements. An additional benefit of the Nokomis sites was their close proximity to a recently abandoned, continuously operating tide gauge operated by the county government. Due to time and budget constraints a single tide gauge was determined to be sufficient for the initial tests instead of the array of gauges that would provide more

detailed data for the MHW datum model. The tide level was determined by measuring down to the water from a benchmark disk at the tide gauge site before and after each data collection period.

Mangrove Coastline Testing

Of the three sites selected, Site 1 is the largest site. Figure 4-13 indicates the location of Site 1. The site consists of an island that is a public park with a shoreline that varies between low mangroves and sandy slopes stabilized with some concrete debris. The height of the mangroves is less than the reach of the UAV Simulator Boom but the seaward edge of the mangroves is beyond the reach of the imaging system.

The site conditions allowed for the collection of a swath of imagery consisting of two parallel rows with approximately 350 images each. Forward overlap and sidelap are nominally 80% and 50% respectively. The result is stereo imagery coverage of a strip approximately 250 m long and 7 m wide that includes the MHWL. Two virtually identical datasets were collected at Site 1; one coincided with the lowest tide of the day and the second coincided with the highest tide. Comparison of the imagery from the two datasets will allow a determination to be made as to the value of tide coordinated imagery for determination of intertidal zone elevation data with the CARS system.

Vehicle ground speed and the frame rate of the camera determine the amount of overlap in the images. The formula used to determine the appropriate number of FPS is as follows:

$$n = \frac{v}{w} \tag{4-2}$$

Where
v is the vehicles ground speed, m/s (note: 1 m/s= 3.6 km/h)

and

$$w = \frac{4.8}{f}(1 - O)H \tag{4-3}$$

Where
f is the lens focal length, mm
O is the percent of desired overlap between images
H is height above ground of the lens focal point, m

Therefore, the required number of FPS to achieve the 80% forward overlap desired while maintaining an 8 km/h ground speed (idle speed in 1st gear with clutch fully disengaged) is 3 FPS; this value was used for collection of all four datasets in the coastal study and is illustrated in Figure 4-15.

Bare Earth Testing

Site 2 consists of a gentle slope of coarse sand and shell with a few rock outcroppings. Figure 4-13 indicates the location of Site 2. Obstructions constrained the area of data collection but the shallow slope allowed for four parallel strips of imagery to be acquired within the intertidal zone. The result is a stereo imagery coverage area approximately 30 m long and 14 m wide.

Despite the gentle slope, natural processes created relief of several centimeters within the intertidal zone and the off-road capabilities of the Jeep carrying the UAV Simulator Boom were needed to acquire adequate imagery coverage. The rock outcroppings stabilize the shoreline at Site 2 and the low velocity of the water in the bay makes the shoreline in this area very stable.

Sun Angle Testing

The third site, identified in Figure 4-14, is similar to the second in the slope and ground surface; Site 3 differs from Site 2 in its proximity to the inlet of the bay. Imagery acquisition at Site 3 was conducted at 7:00 am to determine the effects of a very low

sun angle on the image quality. Future research may also benefit from the baseline data collected at Site 3 and the 1.5 km distance between Site 1 and Site 3 provides the opportunity to observe the delay of tidal influence between the inlet and areas further inland.

A very smooth ground surface leading from above the high-tide line and down into the water made Site 3 ideal for imagery acquisition from the ground-based vehicle. The movement of the aerial sensors simulated the dynamics of a UAV platform closely at Site 3, whereas, at the other sites the rough terrain imposed more rapid accelerations than the completed system will experience on a UAV. Even at 50 Hz bandwidth from the IMU the orientation of the image sensor may vary significantly between the sampled instance and image acquisition time; this results in a decrease in accuracy during highly dynamic maneuvers.

Table 4-1. CARS GPS error statistics

Error	ΔEasting	ΔNorthing	ΔHeight
Mean	0.004	-0.001	0.003
Stdev	0.011	0.008	0.023
RMS	0.012	0.008	0.023
Max	0.031	0.027	0.102
Min	-0.103	-0.030	-0.077

Table 4-2. Horizontal position errors of the antenna testing campaign

Error [m]	DN	DE	DN	DE	DN	DE	DN	DE	DN	DE
Test Duration [min]	**15**		**30**		**60**		**120**		**180**	
Antenna Test 1										
Consumer Grade	0.006	-0.004	0.081	-0.020	0.007	-0.003	0.005	-0.004	0.066	0.460
Mapping Grade	-0.085	-0.210	0.000	0.003	0.001	0.003	0.004	0.000	0.004	0.002
Survey Grade	0.004	0.002	0.007	0.003	0.003	0.001	0.000	0.000	0.000	0.000
Antenna Test 2										
No Ground Plane	0.329	0.463	0.318	0.480	0.276	0.474	0.273	0.495	0.014	0.167
15 cm Ground Plane	-0.085	-0.002	0.006	-0.001	0.004	0.000	0.003	0.002	0.005	0.002
30 cm Ground Plane	2.374	-0.738	2.417	-1.382	2.417	-1.382	2.417	-1.382	2.404	-1.379
Antenna Test 3										
No Ground Plane	0.146	0.132	-0.002	-0.002	-0.007	-0.003	-0.006	-0.002	-0.005	-0.002
8 cm Ground Plane	0.064	0.199	0.035	0.223	0.018	0.214	0.034	0.205	0.030	0.203
11 cm Ground Plane	0.003	0.002	-0.002	0.003	-0.004	0.000	-0.002	0.001	0.001	0.002
15 cm Ground Plane	-0.087	0.024	0.001	0.003	0.003	-0.001	NA	NA	NA	NA

Legend
Green: good fixed integer ambiguity solution
Magenta: bad fixed integer ambiguity solution
Yellow: float ambiguity solution
Red: surprisingly bad float ambiguity solution

Table 4-3. CARS IMU gyro drift performance

Channel	Offset (°/s)	σ (°/s)
x	-0.26	0.61
y	-0.79	0.43
z	0.47	0.42

Figure 4-1. Control network of the CARS test range (image from Alachua County Property Appraiser and location sketch from Google Maps)

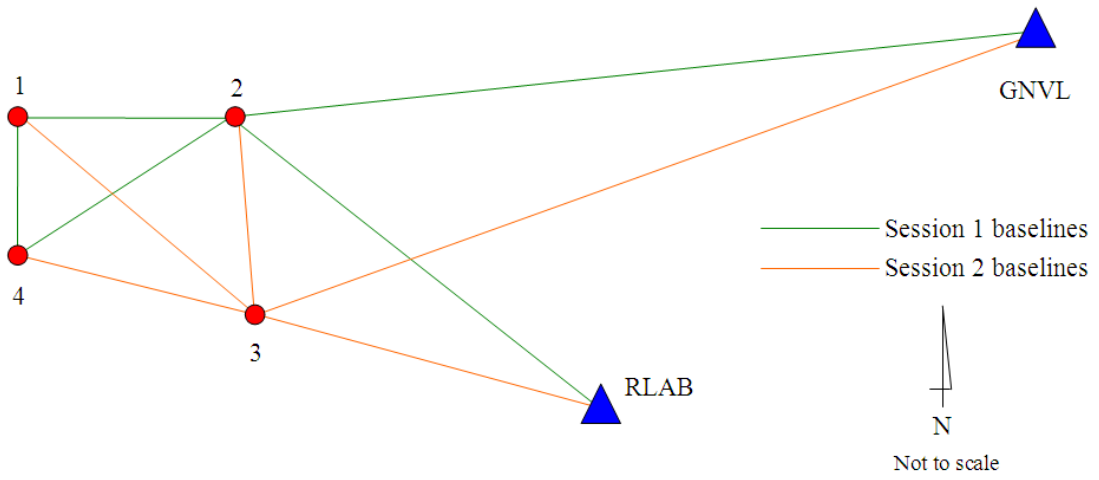

Figure 4-2. Control network baselines of the CARS test range

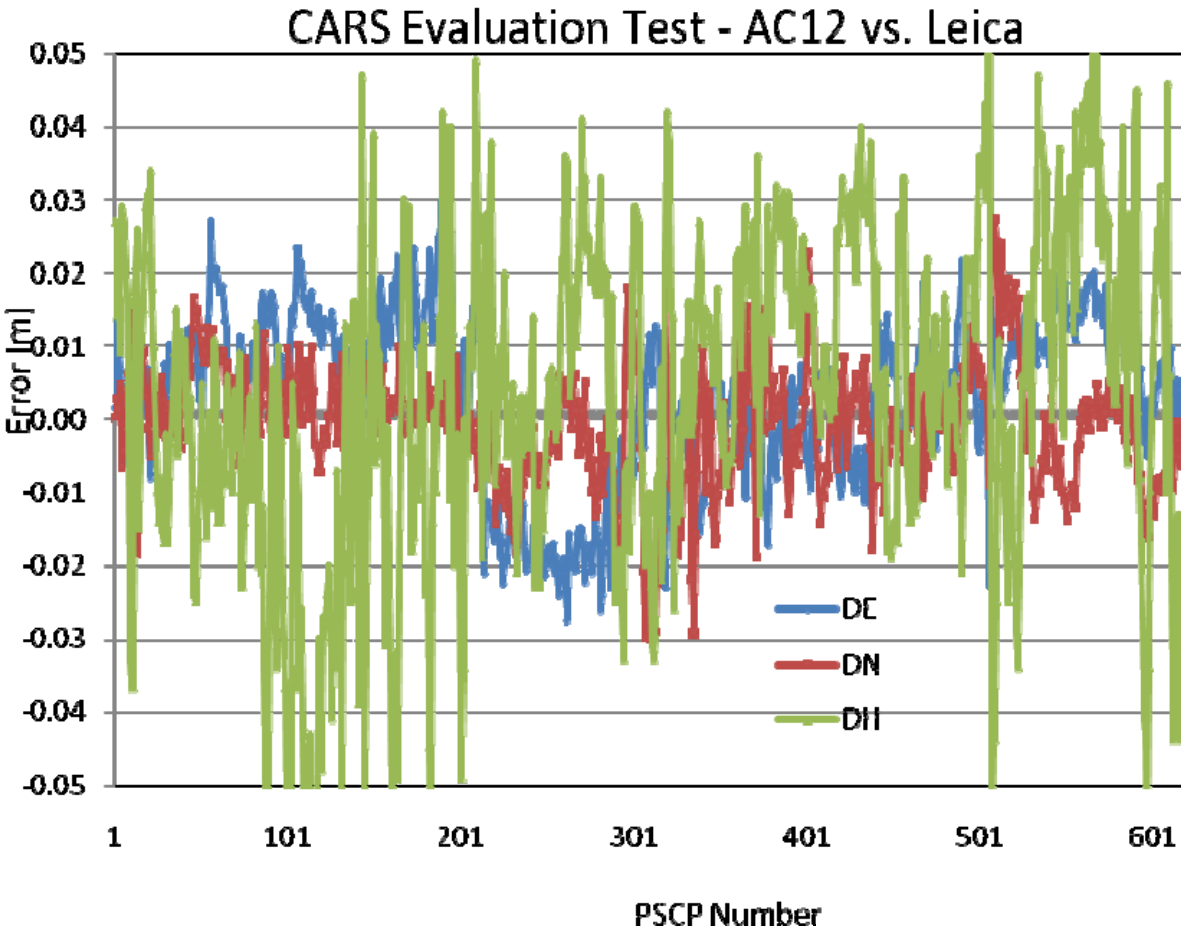

Figure 4-3. CARS AC12 GPS receiver performance

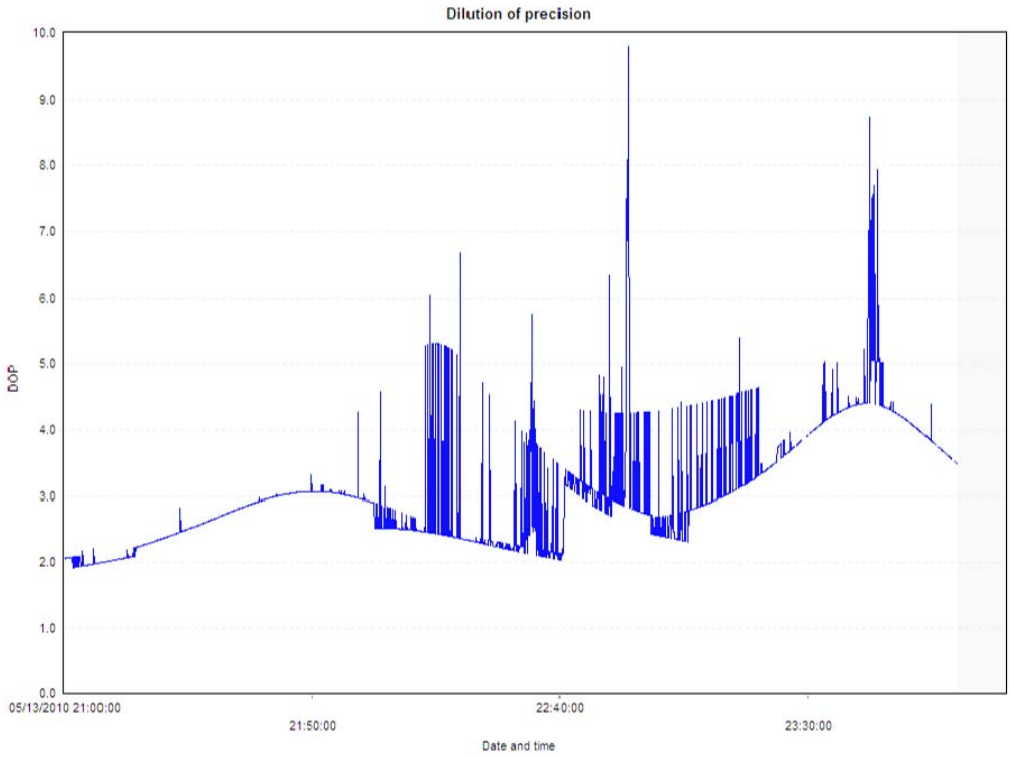

Figure 4-4. Satellite configuration over 90 minute session using GPS patch antenna

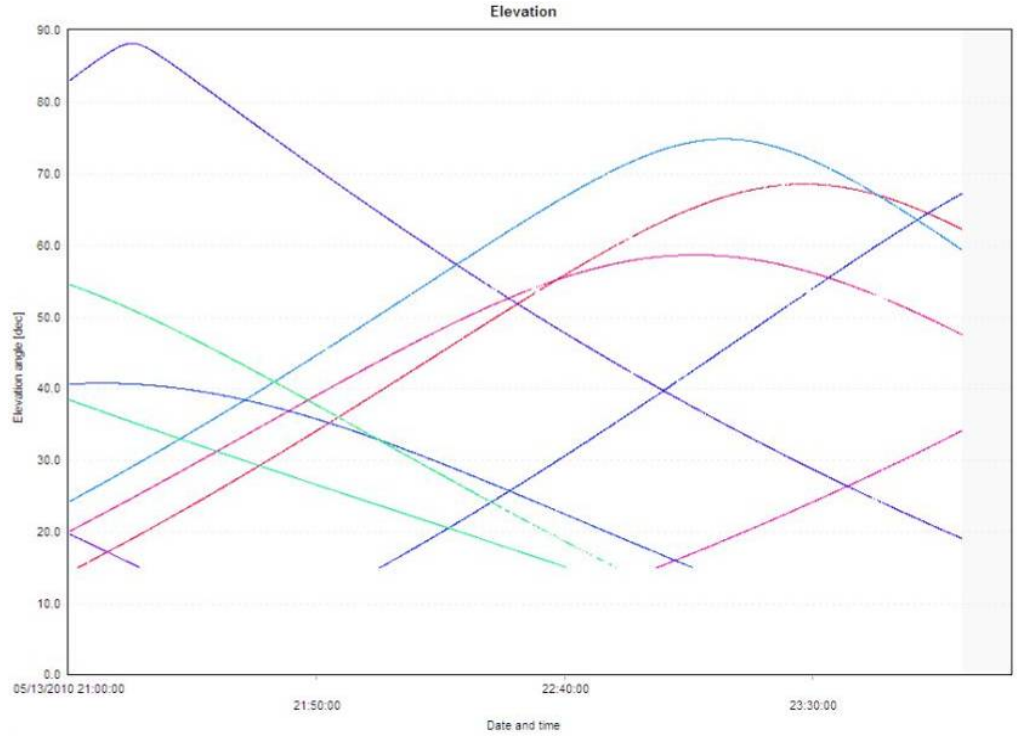

Figure 4-5. Elevation angle of satellites from 90 minute patch antenna session

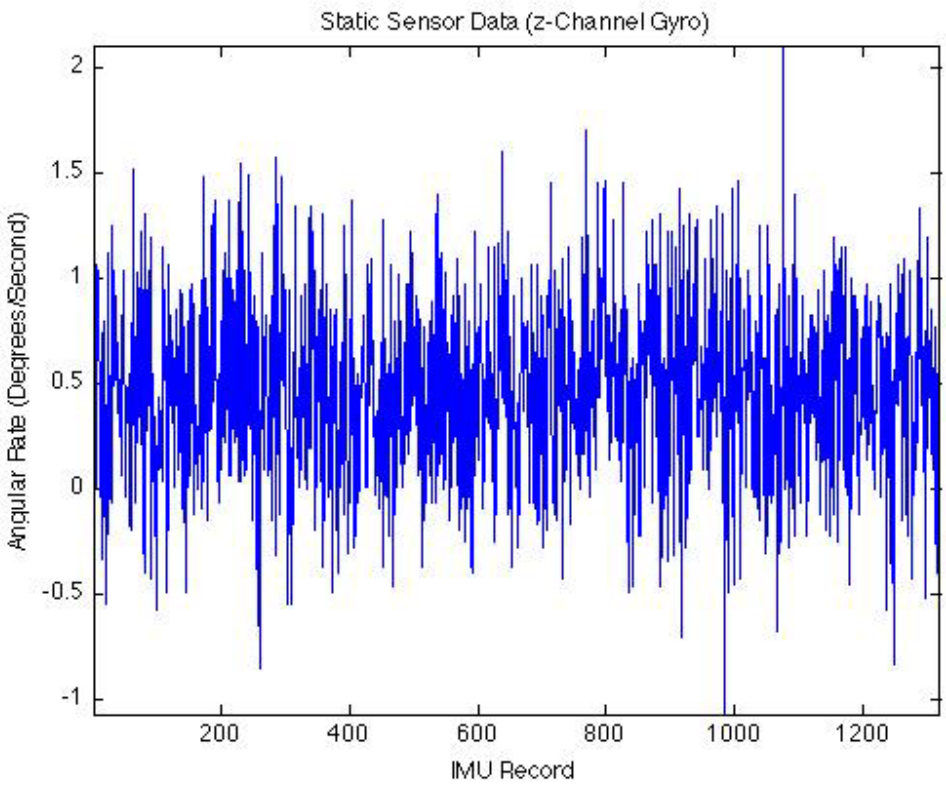

Figure 4-6. nIMU z-Gyro Noise Characteristics

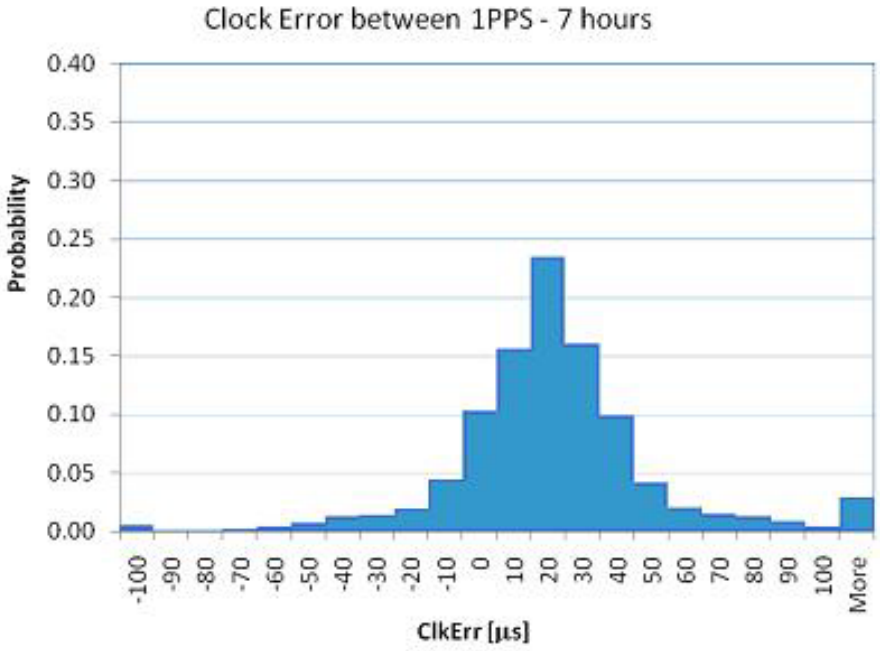

Figure 4-7. GPS/IMU sychronization Clock noise charecteristics

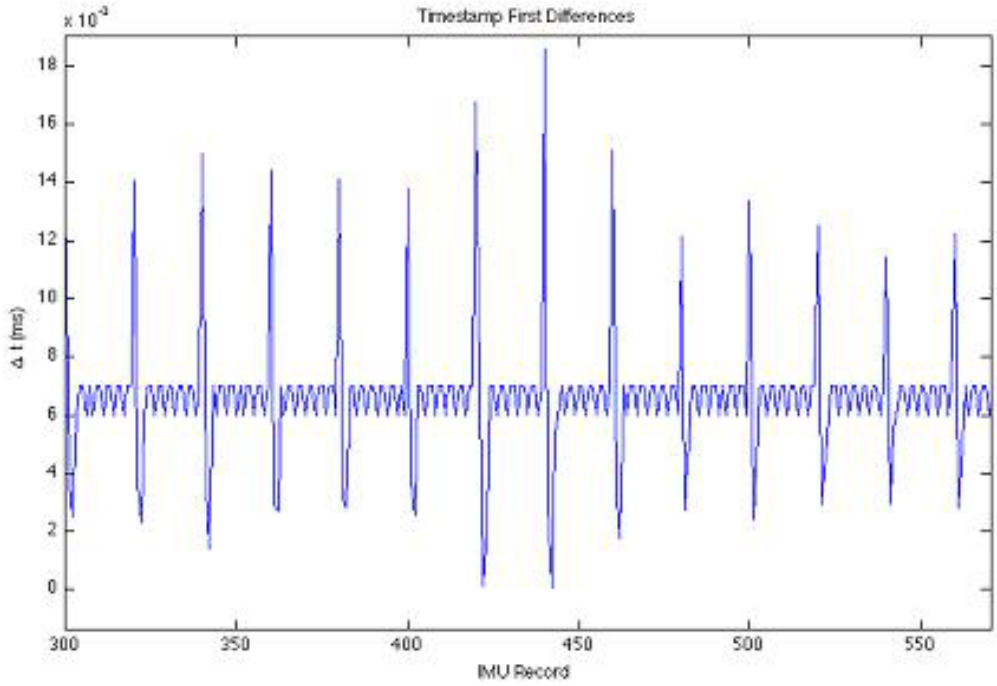

Figure 4-8. GPS/IMU sychronization Clock jitter charecteristics

Figure 4-9. UAV Simulator Boom (image by author)

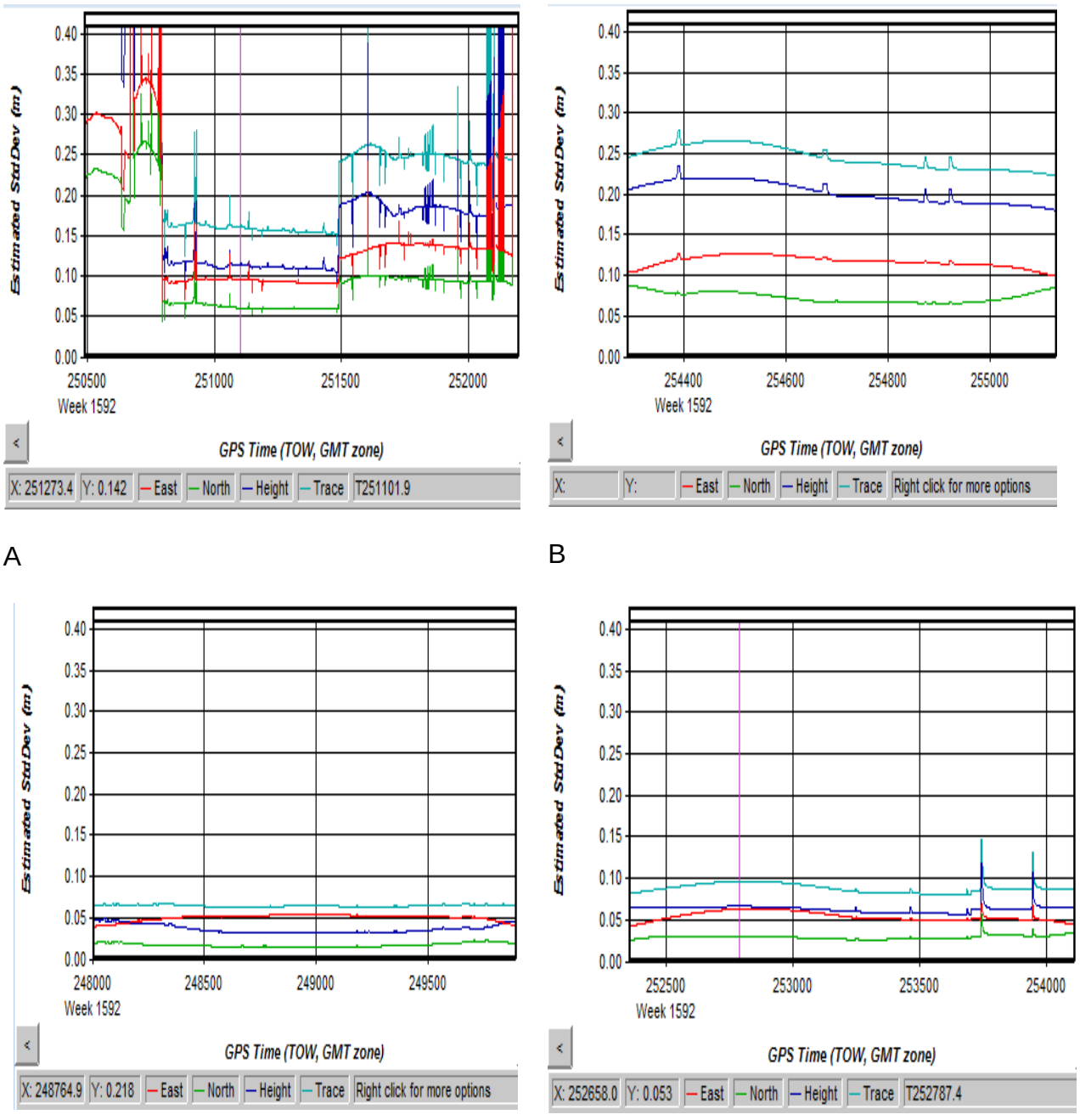

Figure 4-10. Precision of the CARS GPS trajectory. A) Patch antenna with no ground plane. B) Patch antenna with ground plane (short static initialization). C) with Trimble antenna. D) patch antenna with ground plane (sufficient static initialization).

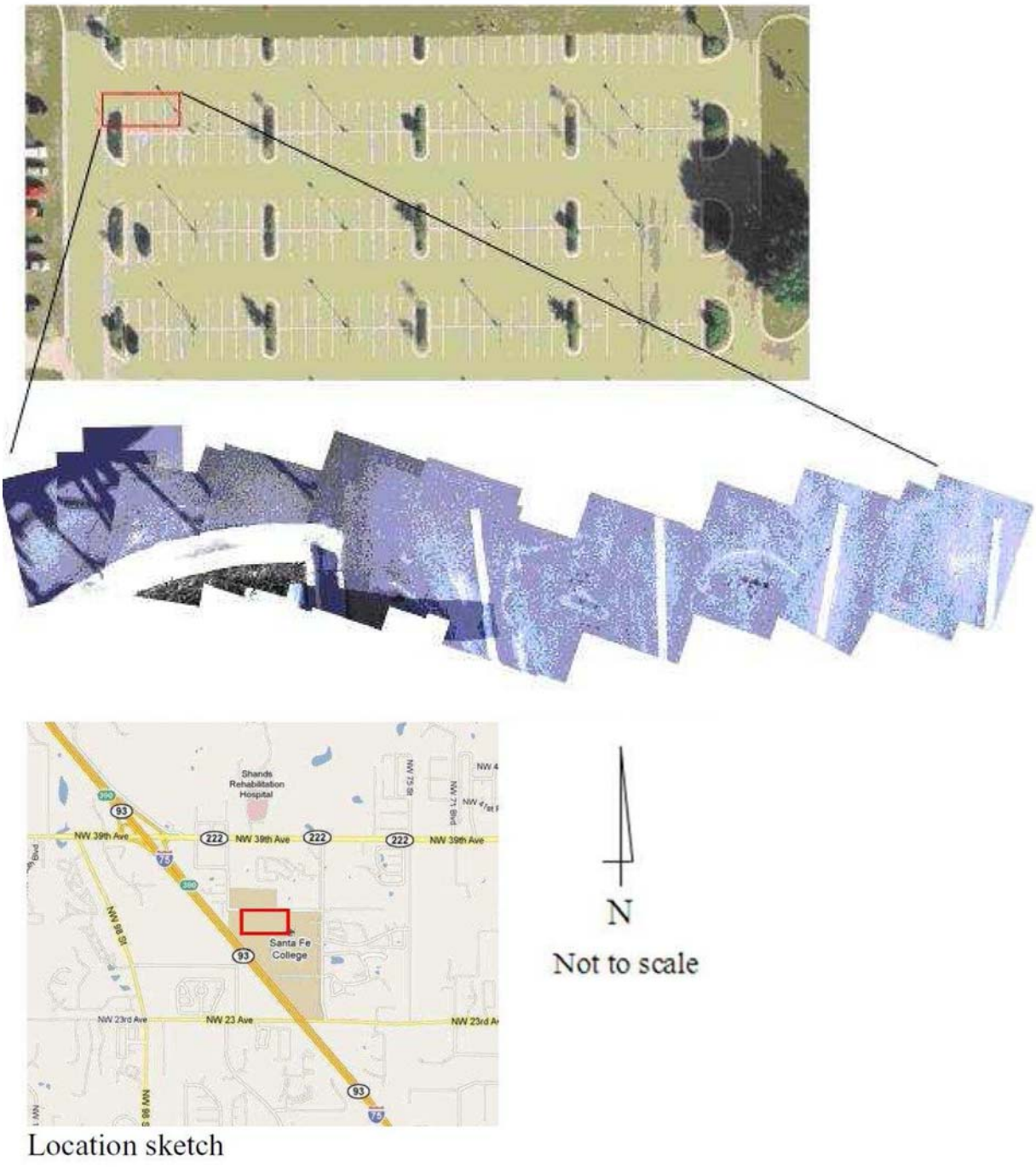

Figure 4-11. Sample of uncorrected CARS imagery of the test range (background image from Alachua County Property Appraiser, foreground images by author, and location sketch from Google Maps)

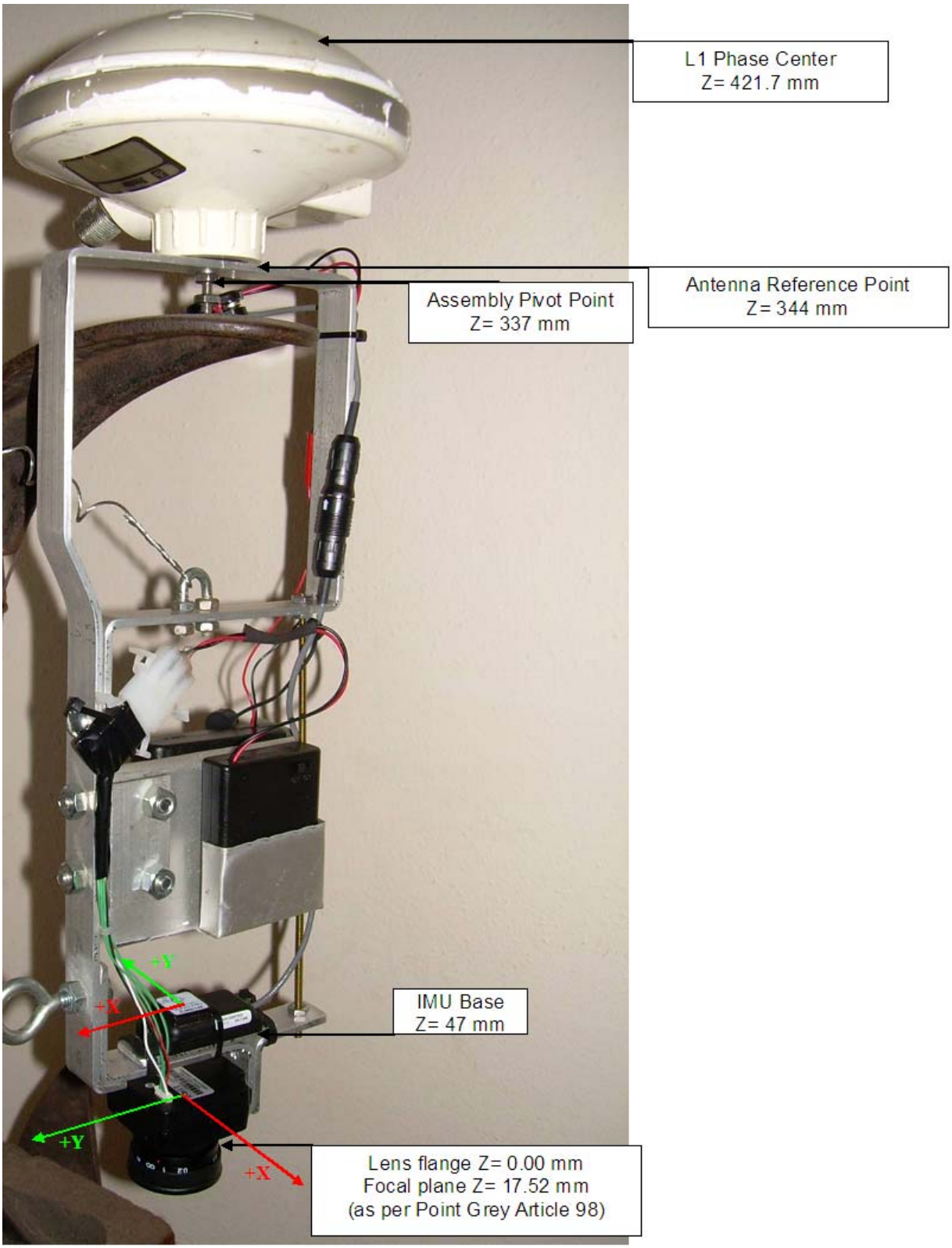

Figure 4-12. CARS aerial assembly with coordinate system axes and offsets (image by author)

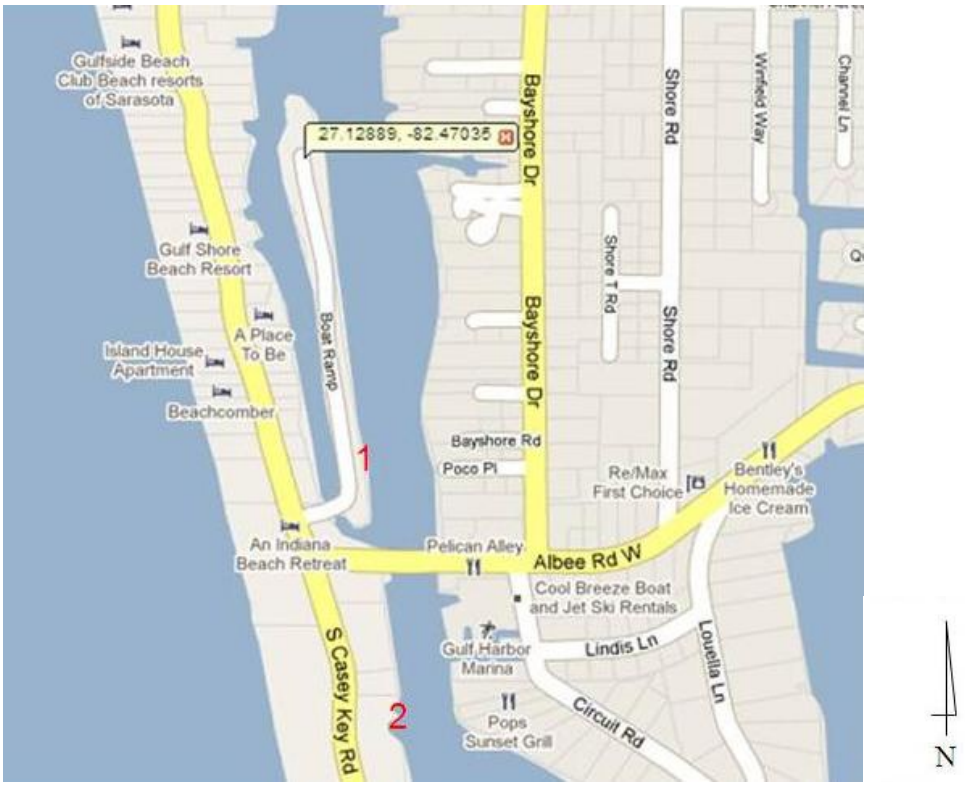

Figure 4-13. Coastal study Site 1 and Site 2 (image from Google Maps)

Figure 4-14. Coastal study Site 3 (image from Google Maps)

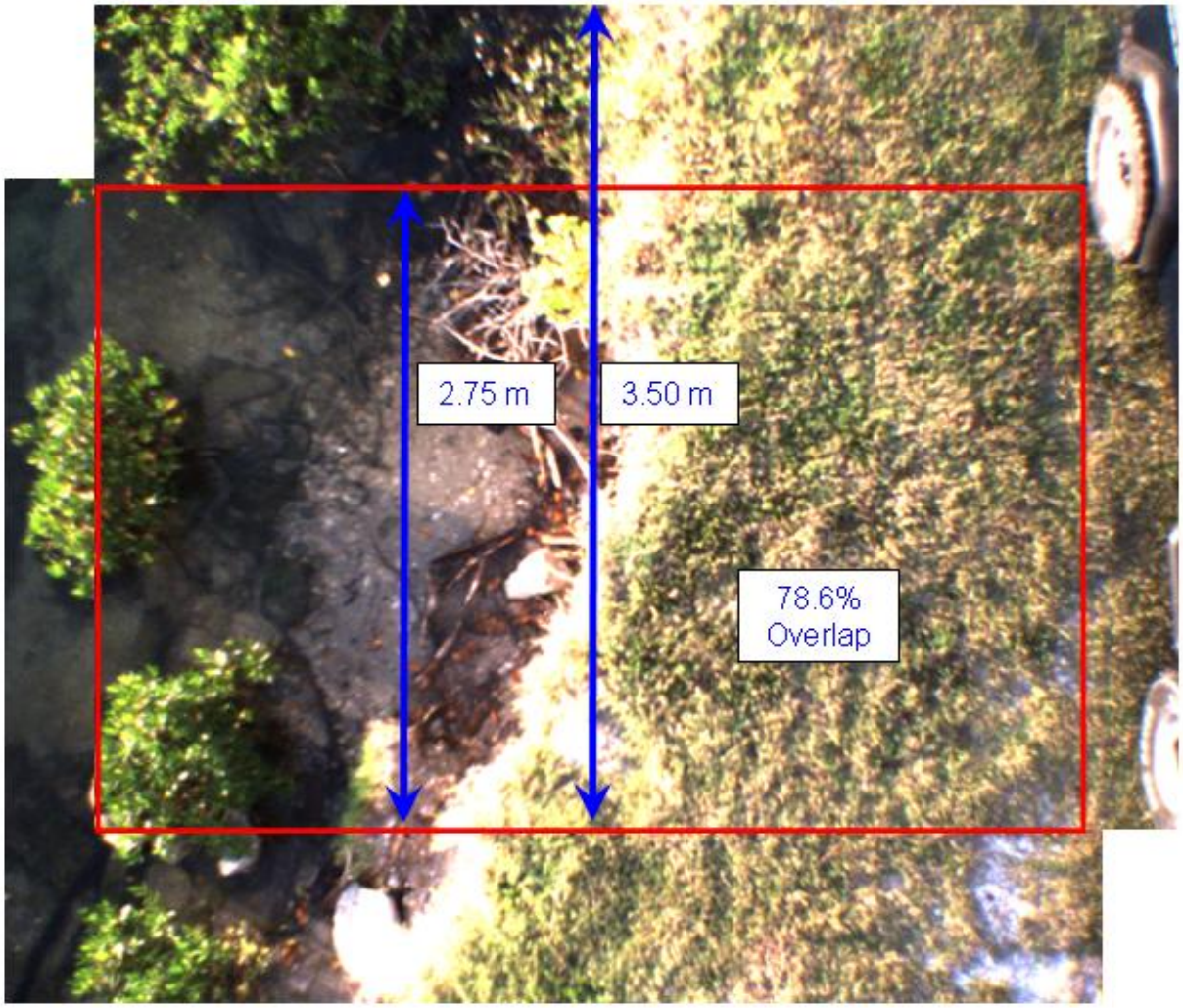

Figure 4-15. Example of CARS imagery showing forward overlap (images by author)

CHAPTER 5
SUMMARY AND CONCLUSIONS

Summary

SLR is a major threat to coastal communities. Current technology cannot provide the data needed to determine the impacts of 36 mm of SLR inexpensively. The ability to evaluate the migration of the MHWL at such a fine resolution will provide communities with valuable information for planning purposes. The MHWL defines the legal boundary between public and private land ownership in Florida and many other states. On the shallow slopes typical to many coastal regions a small vertical rise equates to a large horizontal shift in the MHWL. This study investigates a combination of a precise MHW tidal datum and a terrain model defined by photogrammetric techniques to map the MHWL. The method uses a simple intersection algorithm to determine where the terrain model and the tidal datum meet, thus delineating the MHWL.

An estimate of the contributing factors to the 36 mm error budget for determining the effects of SLR on a 20 year timescale indicates aerial imagery acquired by a remote sensing system on a UAV can meet the intended goal. I demonstrate a need for this level of detail when mapping the MHWL and that existing data are insufficient to provide the necessary detail.

The development and testing of a low-cost, easily deployable, Close-range Aerial Remote Sensing (CARS) system capable of obtaining geodetic-grade elevation data was presented. The preliminary results are within the specifications required to map the effects of SLR on a 20 year timescale.

Two low-cost single frequency GPS receivers capable of acquiring carrier phase raw measurements, the u-blox LEA-5T and the Magellan AC12 were tested. The AC12 performed well in static and kinematic cases and the accuracy requirement for monitoring SLR on a 20 year timescale was met. The CARS system is intended for small vehicles and weight, size, and power consumption are paramount; target gross weight, size, and power consumption of the system are under 500 gm, 30 cm3, and five watts, respectively. After extensive testing, a small commercial patch antenna was proven effective when a suitable ground plane is added. A miniature IMU was also tested to provide the orientation information of the imaging sensor. Lab testing of the IMU confirmed the manufacturer specifications and its suitability to the CARS system. A low-cost, lightweight camera with a C-mount lens to acquire imagery from low altitude was tested; this testing was performed with a UAV Simulator Boom that allows components of the system to be proven effective prior to miniaturization. The indications are the CARS system will provide stereo imagery sufficient to support the intended goal; that goal is the generation of an intertidal zone DEM accurate enough to produce a map of the MHWL at a resolution within the estimate of sea level rise on a 20 year time scale (36 mm).

Examination of the data acquired at the coastal sites indicates UAV based methods could provide the quantity and quality of information needed for SLR impact assessment on a city or county scale in a reasonable amount of time and at a reasonable cost. At a height of 30 m AGL (4X the height of the study) the CARS system equipped with a 12.5 mm focal length lens will acquire a swath of imagery 11.5

m wide with a GSD of 9 mm. At the 3 FPS and 80% overlap values used in the study, a ground speed of 24 km/h would be possible.

Based on an average flight time of 30 minutes, due to power and data storage limitations, approximately 6 km of coastline could be modeled with each flight. Considering the logistics of deploying the system from different locations and coordinating the flights with low tide conditions, approximately 30 km of coastline could be mapped per day. At this rate the entire 11,098 km interior tidal coastline of Florida could be mapped by a single person in approximately one year.

Conclusions

Variations in the tide level within bays may be greater than 20 years of SLR, resulting in inaccurate predictions. Continuous tide readings are widely spaced and the more densely available values for MHW on tidal benchmarks are based on decades old observations. A high resolution tidal datum needs to be produced from an array of tide gauges to predict the effects of SLR on the MHWL in bays at the 20 year timescale.

The 36 mm error budget of a 20 year SLR analysis is within reach. Advances in the technology and reductions in the cost of GPS receivers and IMUs have made the acquisition of elevation data within the 36 mm error budget of a 20 year SLR analysis within reach at a reasonable cost. Directly georeferenced imagery, automated photogrammetric processes, and improvements in LiDAR will continue to reduce the cost and increase the resolution of coastal elevation data.

A CARS system can provide the needed elevation data. Preliminary testing of the CARS system has met the topographic data acquisition requirements of a 20 year SLR analysis. Future additions to the global navigation satellite systems similar to GPS will allow low cost receivers to perform even better. The FAA will receive more and more

requests for allowances in the use of UAVs and the day will come when CARS systems could provide the information communities need to make critical decisions about development.

The imagery's ability to penetrate mangroves was not proven by the coastal study and much of the coastline may be obstructed from modeling by photogrammetric techniques. Interpolation of elevation data in these areas may be an option. Gaps in the canopy that are large enough to allow for identification of coincident points in stereo imagery may be less frequent than gaps that would allow LiDAR penetration; the accuracy of the points on each end of the interpolated area would likely be more accurate from the CARS system than from high altitude LiDAR, resulting in a more accurate DEM.

Further research needs to be conducted to complete the assessment of the methods proposed in this document. The accuracy obtainable in modeling the tidal datum and the error involved in the photogrammetric process need to be determined before a conclusion can be made as to the fitness of this process to achieving the 36 mm accuracy needed to predict the impacts of SLR at the 20 year timescale.

APPENDIX A
ANTENNA TESTING

Further detail is provided here for the antenna testing described in Charter 4. The most important part of the test focused on the ability to produce centimeter accuracy with a dielectric patch type of antenna. A u-blox ANN-MS, consumer-grade, model 0-005-0 antenna was connected to the AC12 receiver via approximately 20 m of cable to allow the receiver to be mounted inside the building for ease of providing power and data storage capacity on a desktop computer. The u-blox antenna is manufactured with a 5 m cable that is not removable; that required the use of an adapter from an N connector to an SMA connector and made the total cable run approximately 25 m.

The ground planes used in the test are constructed of 22 gauge galvanized steel sheet backed by a piece of hardboard to maintain a flat surface. The four ground planes used are shown in Figure A-1 and they have sizes of 8, 11, 15, and 30 cm. A mount, also in Figure A-1, was constructed to produce the same vertical offset as the ground planes but to provide no benefit to the GPS signals.

Plots of the dilution of precision (DOP) values for the 15 minute observation of each configuration are provided in Figure A-2.

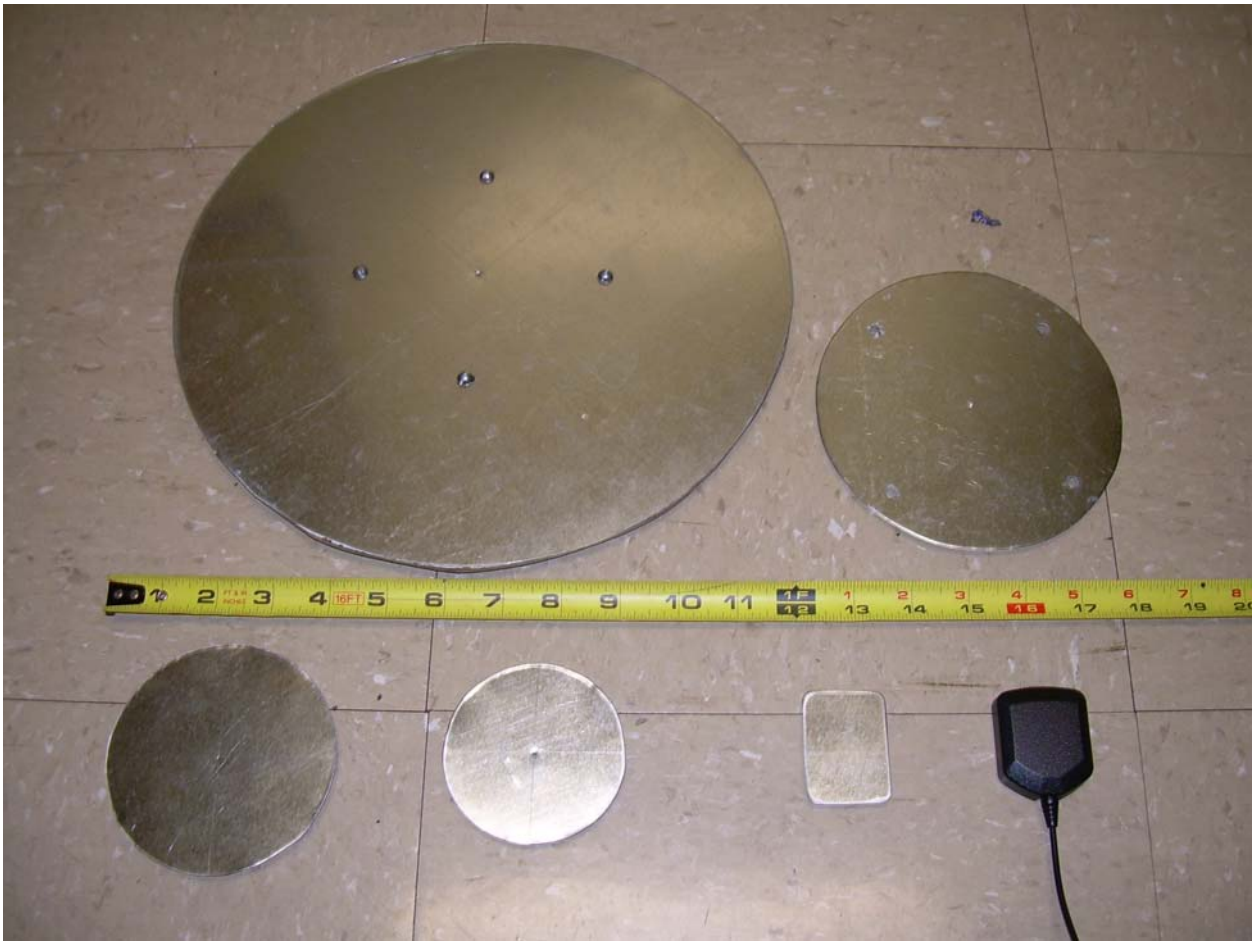

Figure A-1. Ground planes compared during antenna testing (image by author)

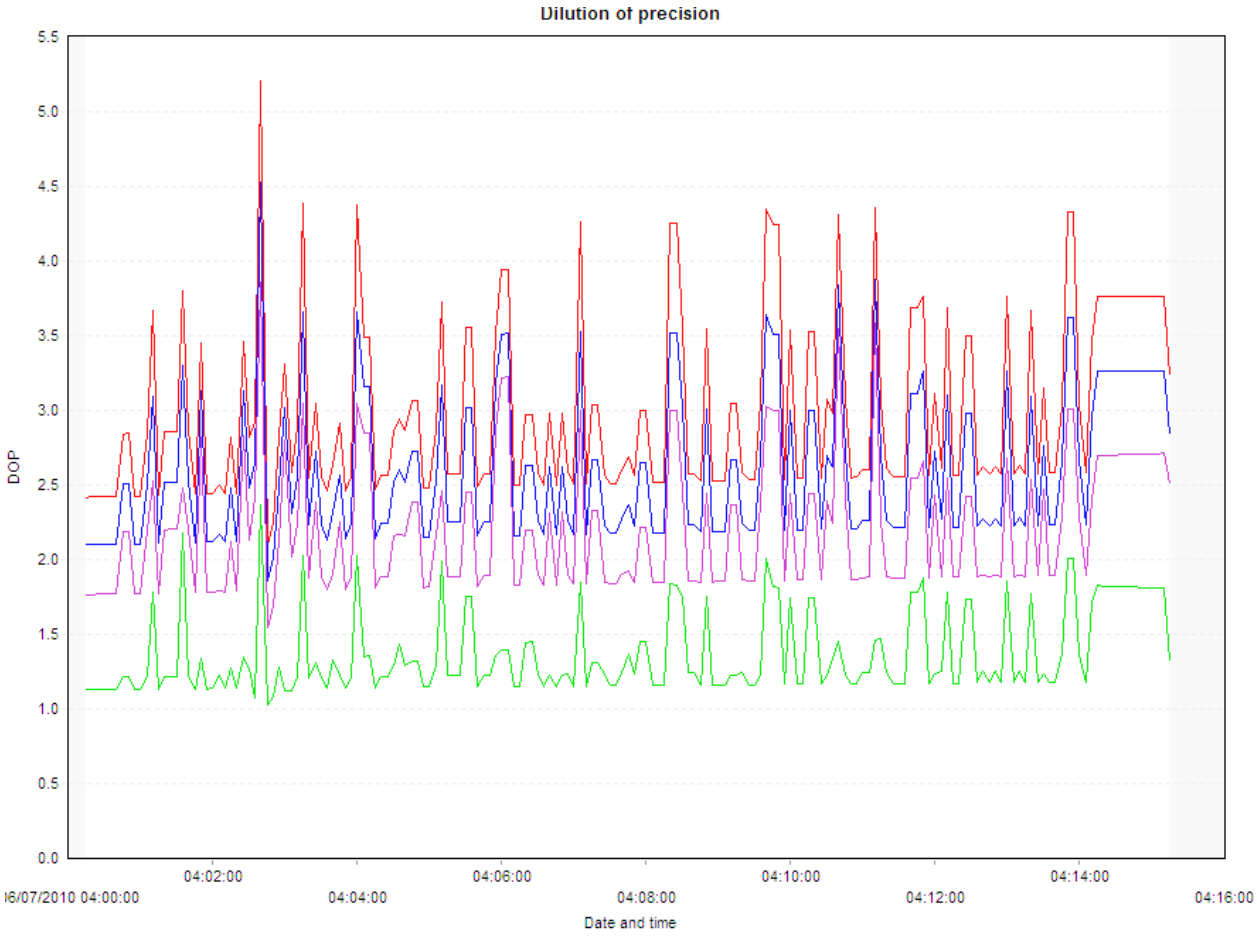

a) no ground plane case

Figure A-2. Effect of ground plane size on GPS signal reception

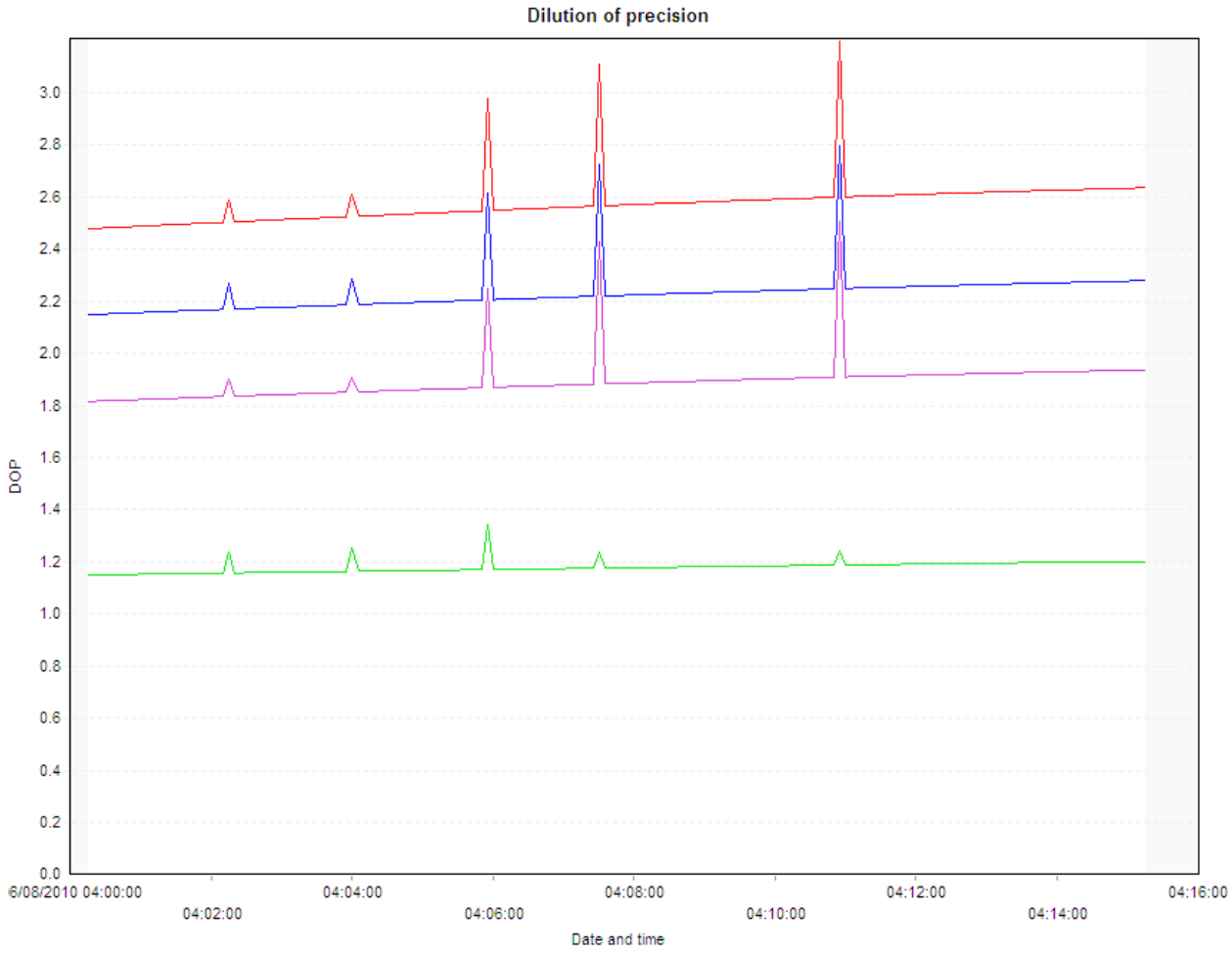

b) 8 cm ground plane case

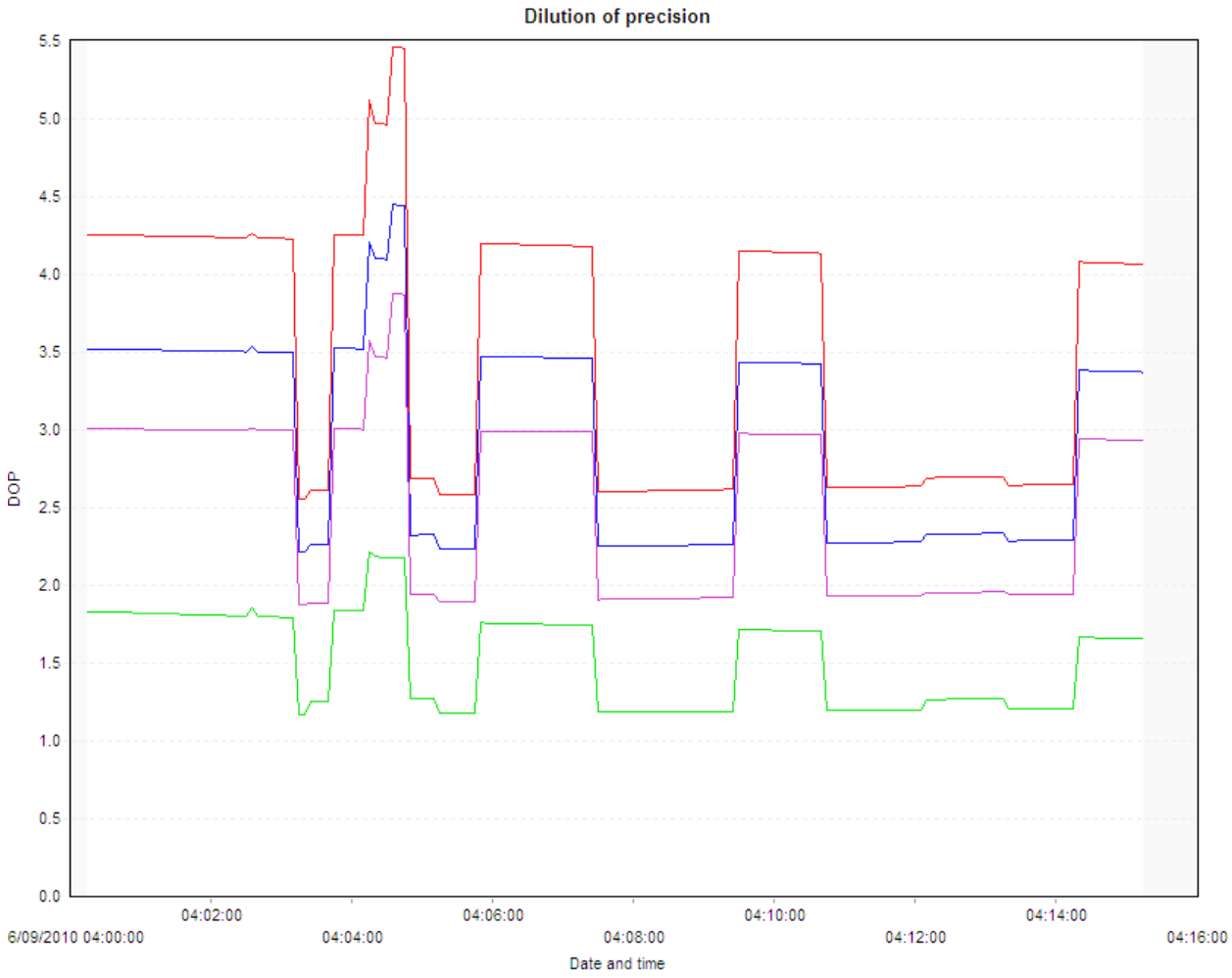

c) 11 cm ground plane case

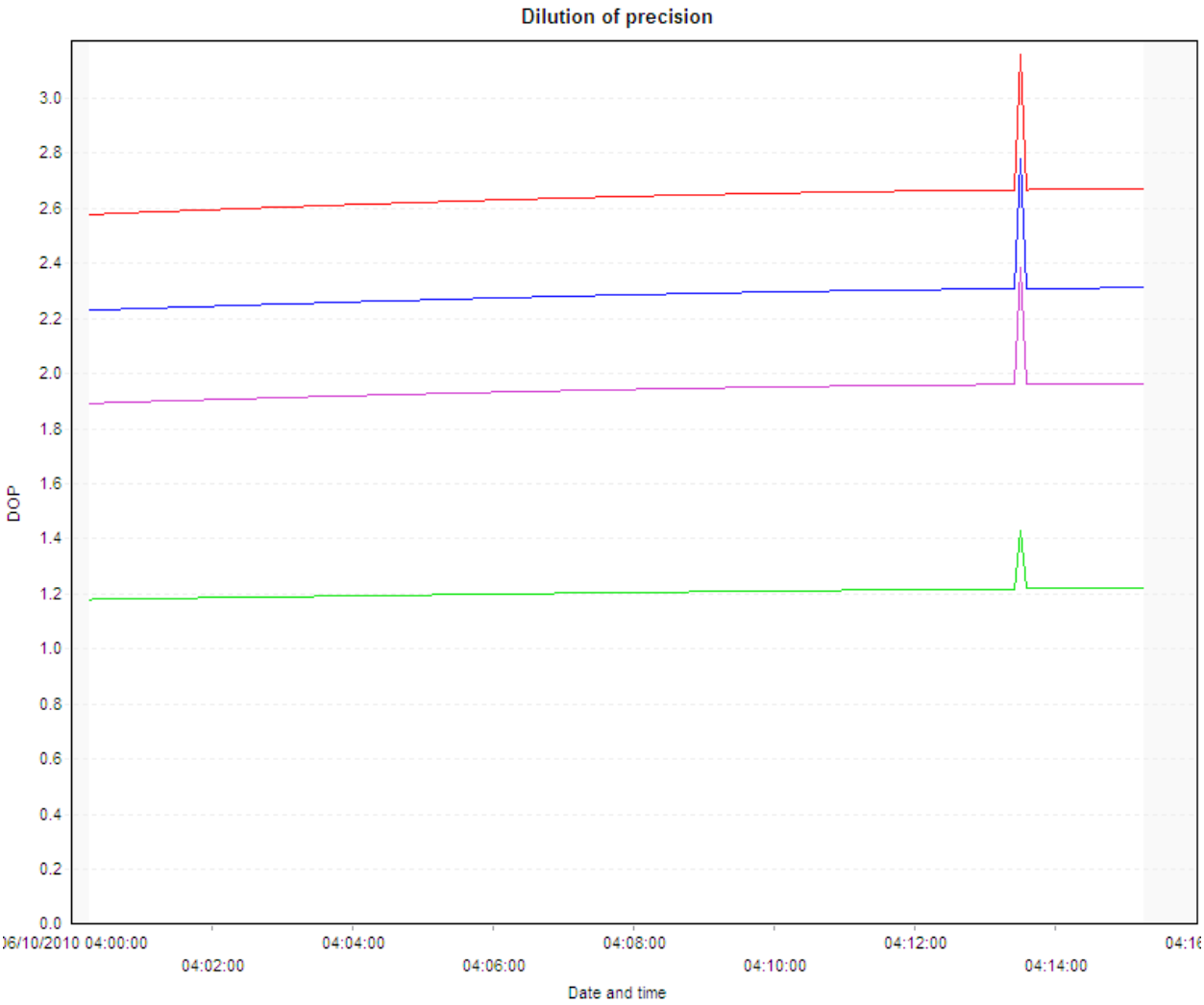

d) 15 cm ground plane case

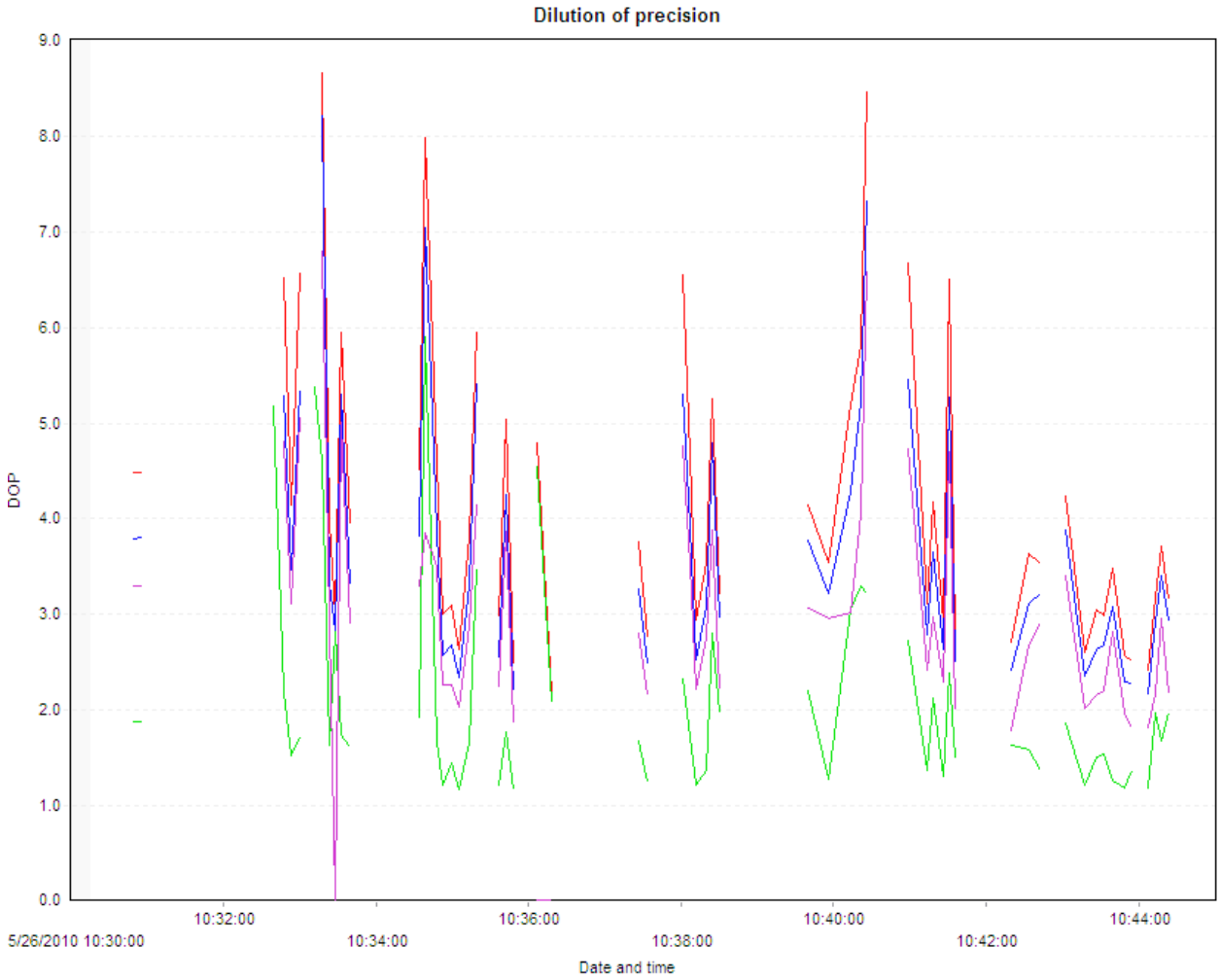

d) 30 cm ground plane case (from an earlier testing window)

APPENDIX B
WESTWARD BIAS INVESTIGATION

The severe westward bias in the solution from the test of the u-blox LEA-5T receiver coupled with past experience with lesser accuracy in the east-west direction than in the north-south direction led to an investigation into dilution of precision (DOP) values. A custom application for calculating the north-south and east-west DOP components separately for GPS observations was used.

For evaluating the phenomenon we have observed of a consistently larger east-west error in GPS observations in the Gainesville, Florida area the following experiment was performed. Four 1 hour GPS observations from each of four Continuously Operating Reference Stations (CORS) around the world were downloaded from the U.S. National Geodetic Survey's website. The datasets are from Julian days 001, 091, 183, and 274 in the year 2009 and span the hour of 0:00 to 1:00 UTC. The four CORS chosen for the test are BRFT, GNVL, ISBA, and PUO1 in Brazil, Florida, Iraq, and Alaska respectively.

The EDOP and NDOP values for each one-second epoch were calculated. Each of the 3600 values for each station per day were averaged and entered into Table B-1. Each of the four daily averages per station was then averaged to obtain the most probable value of EDOP and NDOP in a represented region of the world. The average values for each day for all four stations and the average of days and stations combined were calculated as well. The ratio of the EDOP to the NDOP was then calculated for each combination.

Results from the analysis indicate there is a statistically significant difference in the north-south and east-west satellite geometry over Gainesville when compared with the

other three sites. As can be seen in Figure B-1, Gainesville has by far the largest ratio between the EDOP and NDOP values and the observed phenomenon of lesser accuracy in the east-west direction is actually reversed at the Iraq and Alaska sites.

Graphs of the individual epoch values are provided in Figure B-2.

Table B-1. East and North DOP in four regions of the world

Site	EDOP	NDOP	Ratio
BRFT001	0.90	0.72	1.24
BRFT091	1.15	0.86	1.34
BRFT183	0.91	0.81	1.12
BRFT274	0.97	0.84	1.16
GNVL001	1.01	0.52	1.96
GNVL091	1.02	0.73	1.39
GNVL183	1.06	0.77	1.37
GNVL274	1.25	0.78	1.60
ISBA001	0.65	0.87	0.74
ISBA091	0.88	0.76	1.15
ISBA183	0.85	0.96	0.89
ISBA274	0.90	0.76	1.18
PUO1001	0.72	0.88	0.82
PUO1091	0.60	0.83	0.73
PUO1183	0.63	0.82	0.77
PUO1274	0.67	0.84	0.81
Average All	0.89	0.80	1.14
BRFT Average (Brazil)	0.98	0.81	1.22
GNVL Average (Florida)	1.08	0.70	1.55
ISBA Average (Iraq)	0.82	0.84	0.98
PUO1 Average (Alaska)	0.66	0.84	0.78
Day 001 Average	0.82	0.71	1.16
Day 091 Average	0.91	0.84	1.09
Day 183 Average	0.86	0.91	0.95
Day 274 Average	0.95	0.80	1.19

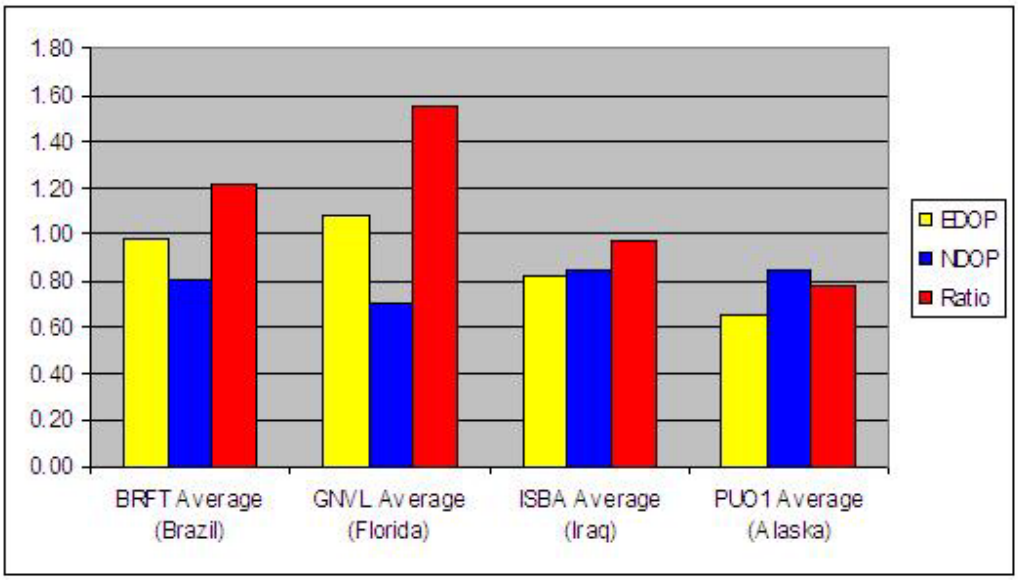

Figure B-1. East and North DOP in four regions of the world

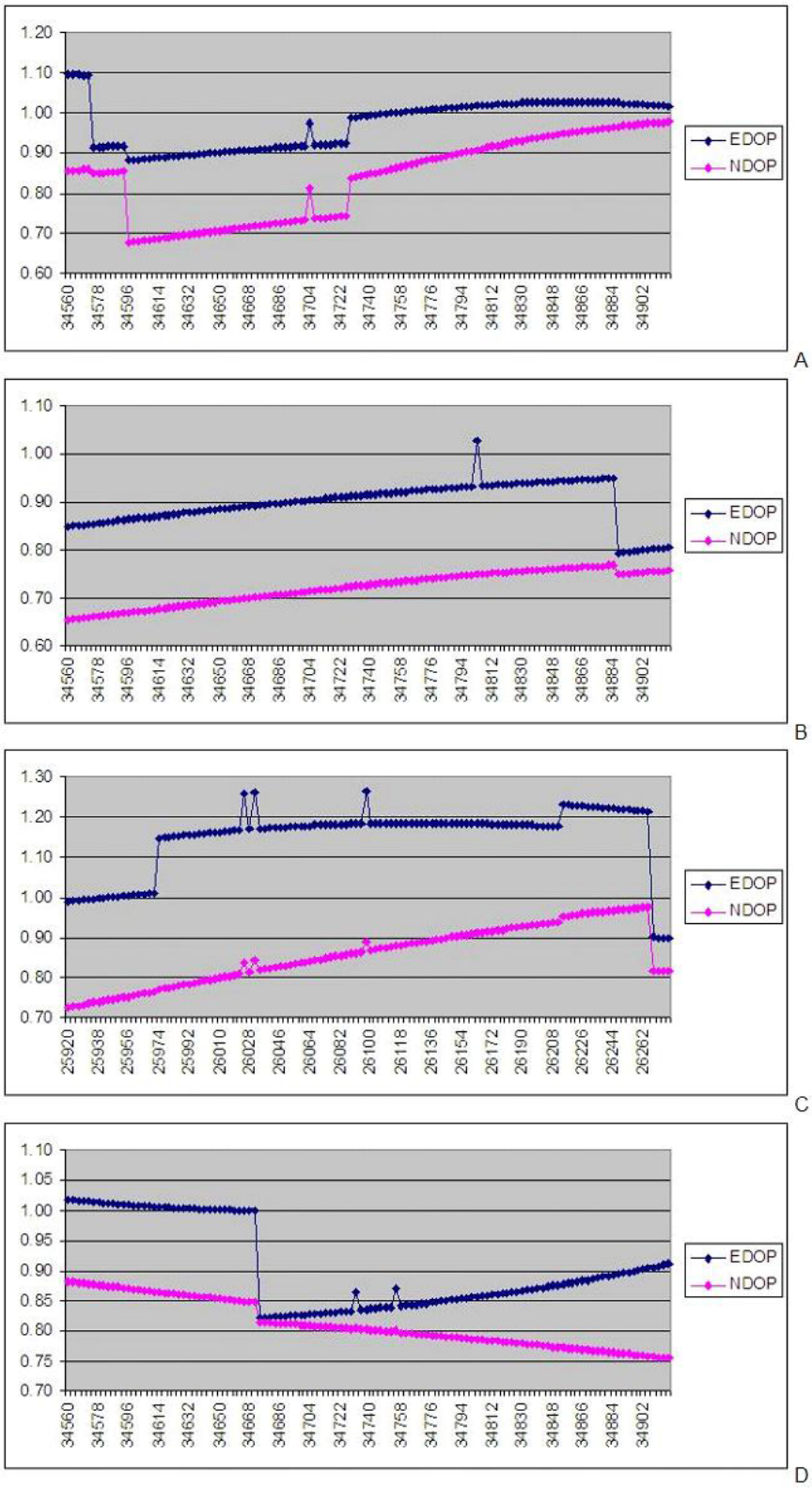

a) CORS BRFT

Figure B-2. East and North DOP values over a year

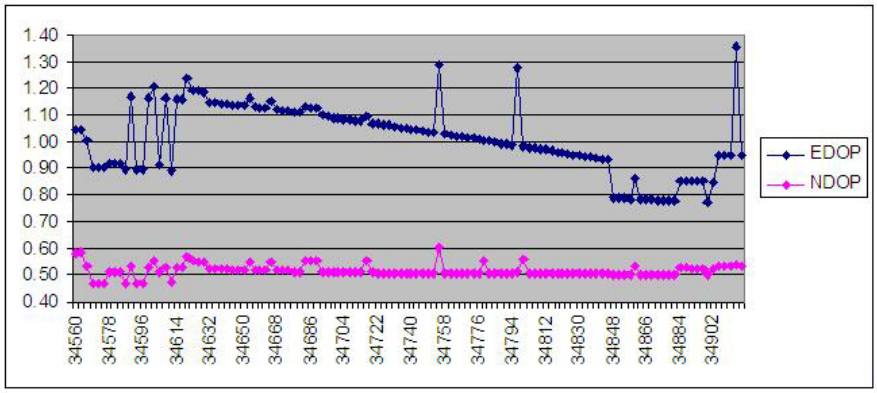

A

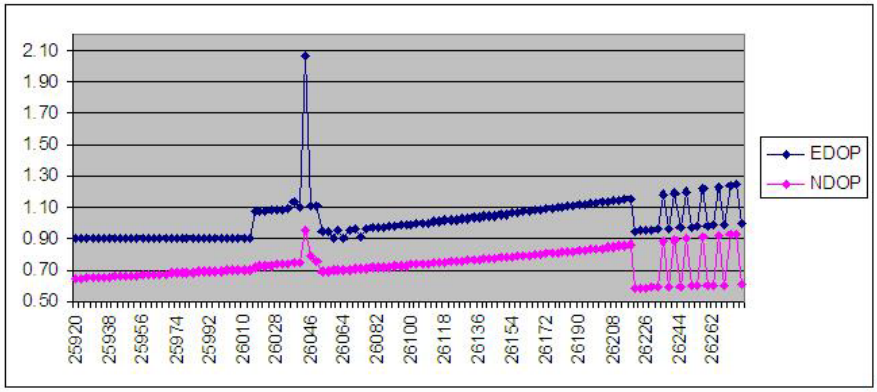

B

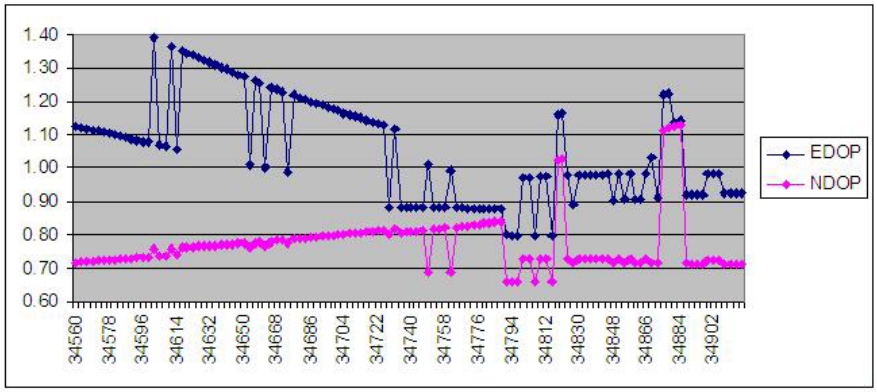

C

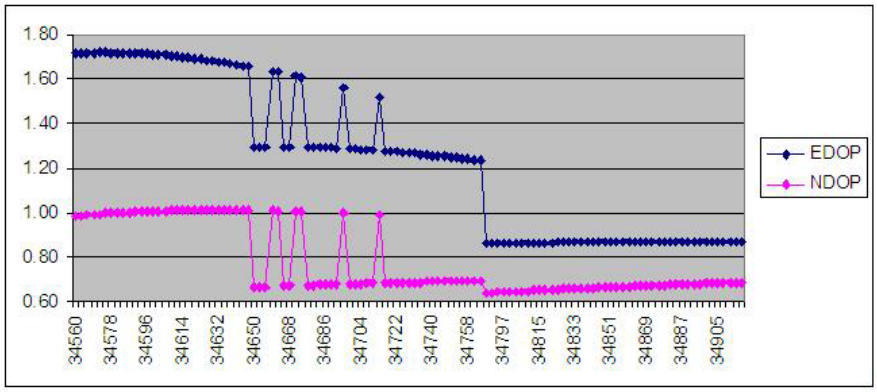

D

b) CORS GNVL

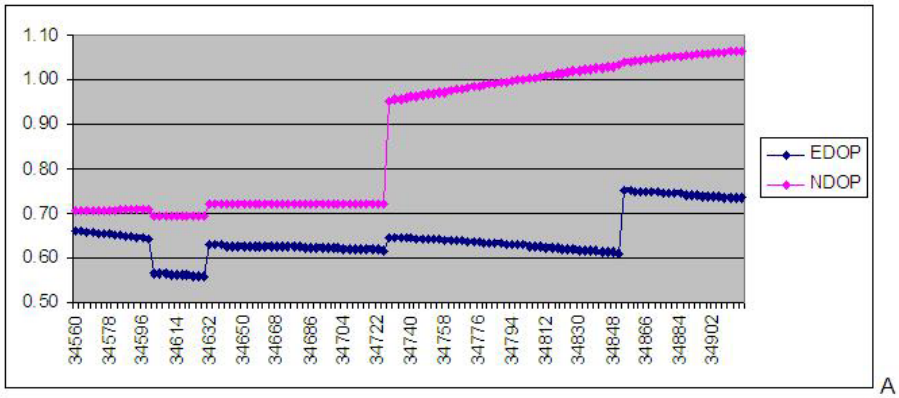

A

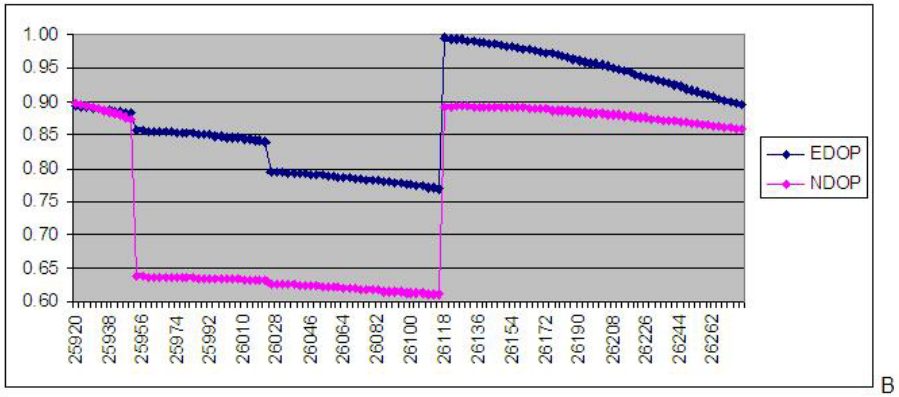

B

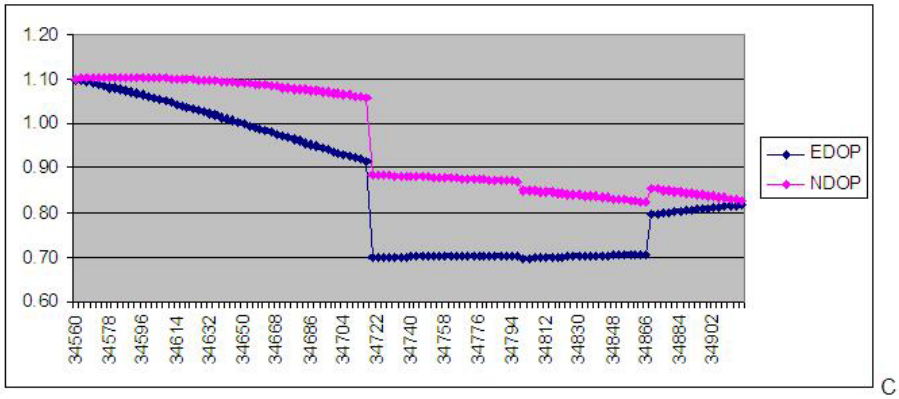

C

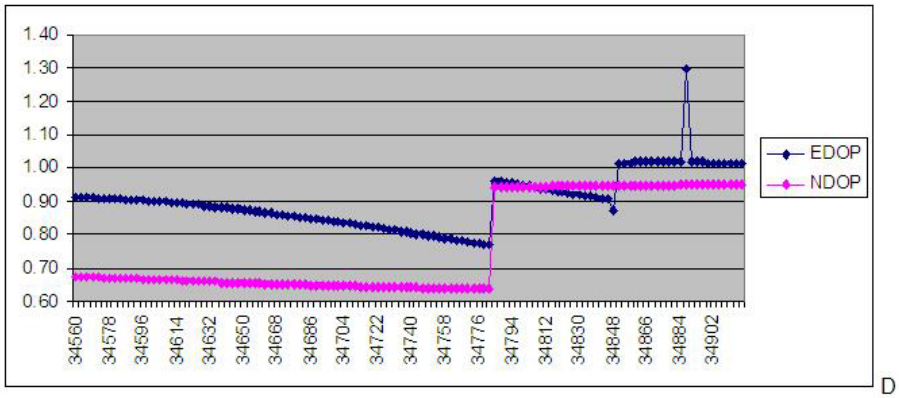

D

c) CORS ISBA

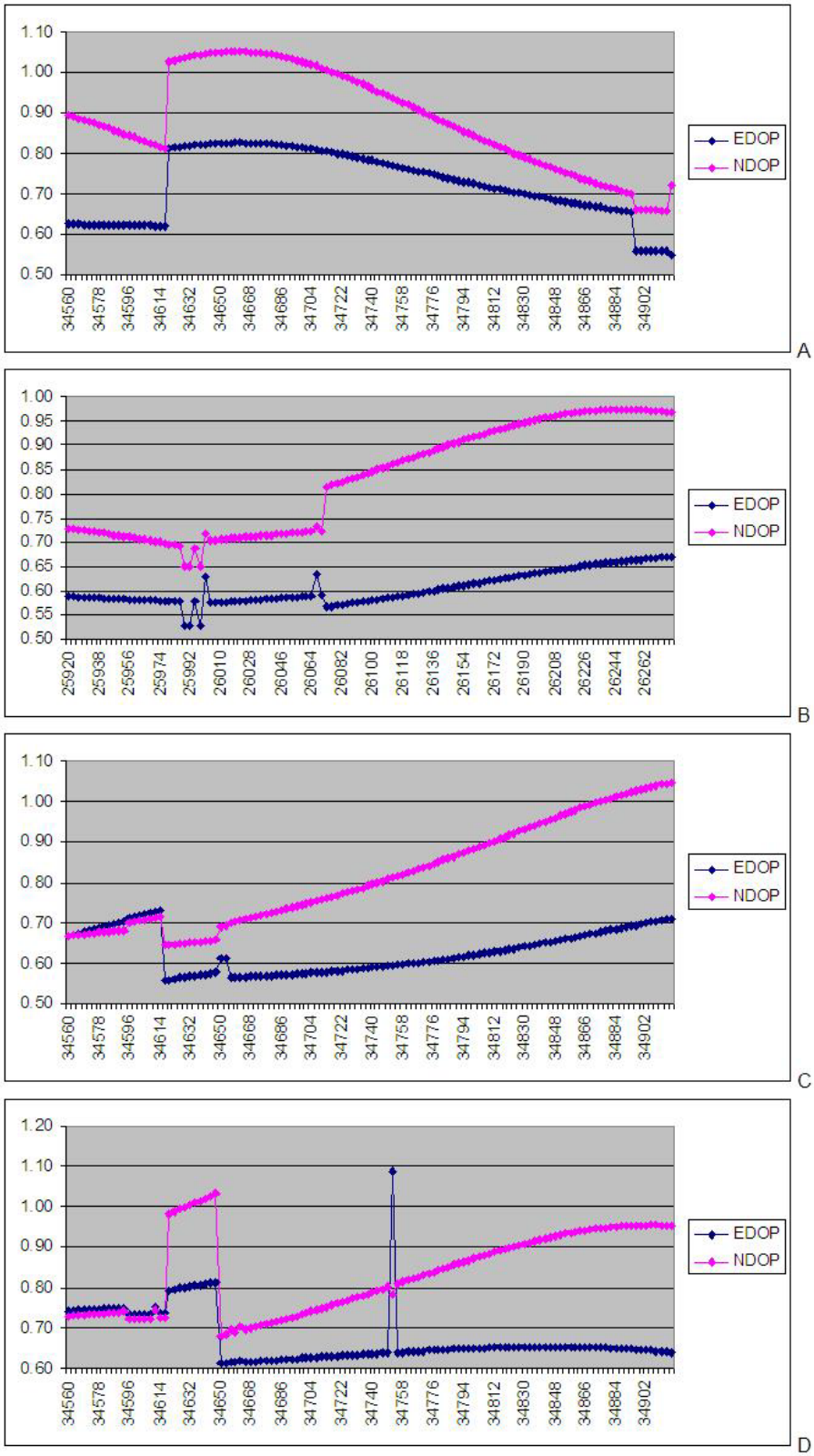
1.10
1.00
0.90
0.80
0.70
0.60
0.50
34560 34578 34596 34614 34632 34650 34668 34686 34704 34722 34740 34758 34776 34794 34812 34830 34848 34866 34884 34902
EDOP
NDOP
A
1.00
0.95
0.90
0.85
0.80
0.75
0.70
0.65
0.60
0.55
0.50
25920 25938 25956 25974 25992 26010 26028 26046 26064 26082 26100 26118 26136 26154 26172 26190 26208 26226 26244 26262
EDOP
NDOP
B
1.10
1.00
0.90
0.80
0.70
0.60
0.50
34560 34578 34596 34614 34632 34650 34668 34686 34704 34722 34740 34758 34776 34794 34812 34830 34848 34866 34884 34902
EDOP
NDOP
C
1.20
1.10
1.00
0.90
0.80
0.70
0.60
34560 34578 34596 34614 34632 34650 34668 34686 34704 34722 34740 34758 34776 34794 34812 34830 34848 34866 34884 34902
EDOP
NDOP
D

d) CORS PUO1

APPENDIX C
BORESIGHT CALIBRATION

Correction of the angular misalignment of the inertial measurement unit (IMU) and the image sensor is accomplished by a boresight calibration. Skaloud (2003) states that a “1-step” procedure can be performed to estimate the boresight angles; this is done “by introducing IMU orientation as additional observations in the bundle adjustment and estimating the boresight as one of its parameters” and comparing the IMU attitude with values obtained by aero-triangulation (AT).

In order to perform such a boresight calibration with the CARS system a dataset was acquired at the test range described in Chapter 4 prior to performing the coastal study. A block of 12 images was selected with 19 ground control points (GCPs) evenly distributed within their footprint. The image coordinates of the GCPs and their corresponding State Plane Coordinate System values are listed in Table C-1.

Figure C-1 illustrates the layout of the boresight calibration layout.

Table C-1. Boresight calibration coordinates.

	Image Coordinates		World Coordinates		
Image	x	y	X	Y	Z
	1129	441	2623517.83	254872.89	179.56
271	1126	480	2623518.30	254872.91	179.58
	1209	9	2623518.30	254872.91	179.58
	1163	705	2623526.88	254873.06	179.45
274	1160	743	2623527.33	254873.08	179.42
	1234	170	2623526.88	254873.06	179.45
	1229	208	2623527.33	254873.08	179.42
	1100	893	2623535.67	254873.05	179.32
276	1094	930	2623536.17	254873.06	179.32
	1192	556	2623535.67	254873.05	179.32
279	1190	596	2623536.17	254873.06	179.32
	1226	174	2623535.67	254873.05	179.32
	1226	211	2623536.17	254873.06	179.32
	1240	924	2623544.81	254873.47	179.14
281	1239	959	2623545.24	254873.50	179.13
	1248	650	2623544.81	254873.47	179.14
282	1245	687	2623545.24	254873.50	179.13
	95	400	2623518.34	254852.89	179.07
	86	364	2623518.38	254853.36	179.07
	122	349	2623517.93	254853.36	179.08
460	133	387	2623517.90	254852.88	179.10
	151	709	2623527.50	254853.01	178.95
	159	750	2623527.51	254853.49	178.94
	189	703	2623527.04	254853.52	178.91
	199	744	2623527.07	254853.04	178.92
	47	31	2623518.34	254852.89	179.07
459	83	23	2623517.90	254852.88	179.10
	158	844	2623536.39	254853.09	178.86
	195	845	2623536.39	254853.58	178.89
	192	808	2623535.89	254853.60	178.88
	154	806	2623535.90	254853.11	178.87
	133	121	2623527.50	254853.01	178.95
	172	118	2623527.51	254853.49	178.94
	172	77	2623527.04	254853.52	178.91
457	134	81	2623527.07	254853.04	178.92
	295	412	2623536.39	254853.09	178.86
	333	411	2623536.39	254853.58	178.89
	334	369	2623535.89	254853.60	178.88
454	294	371	2623535.90	254853.11	178.87
	154	913	2623545.47	254853.19	178.66
	190	919	2623545.51	254853.71	178.66
	190	879	2623545.02	254853.69	178.69
	153	876	2623545.03	254853.22	178.70
	194	168	2623536.39	254853.09	178.86
	232	167	2623536.39	254853.58	178.89
	235	127	2623535.89	254853.60	178.88
453	196	126	2623535.90	254853.11	178.87
	259	617	2623545.47	254853.19	178.66
	296	623	2623545.51	254853.71	178.66
	301	581	2623545.02	254853.69	178.69
451	260	578	2623545.03	254853.22	178.70

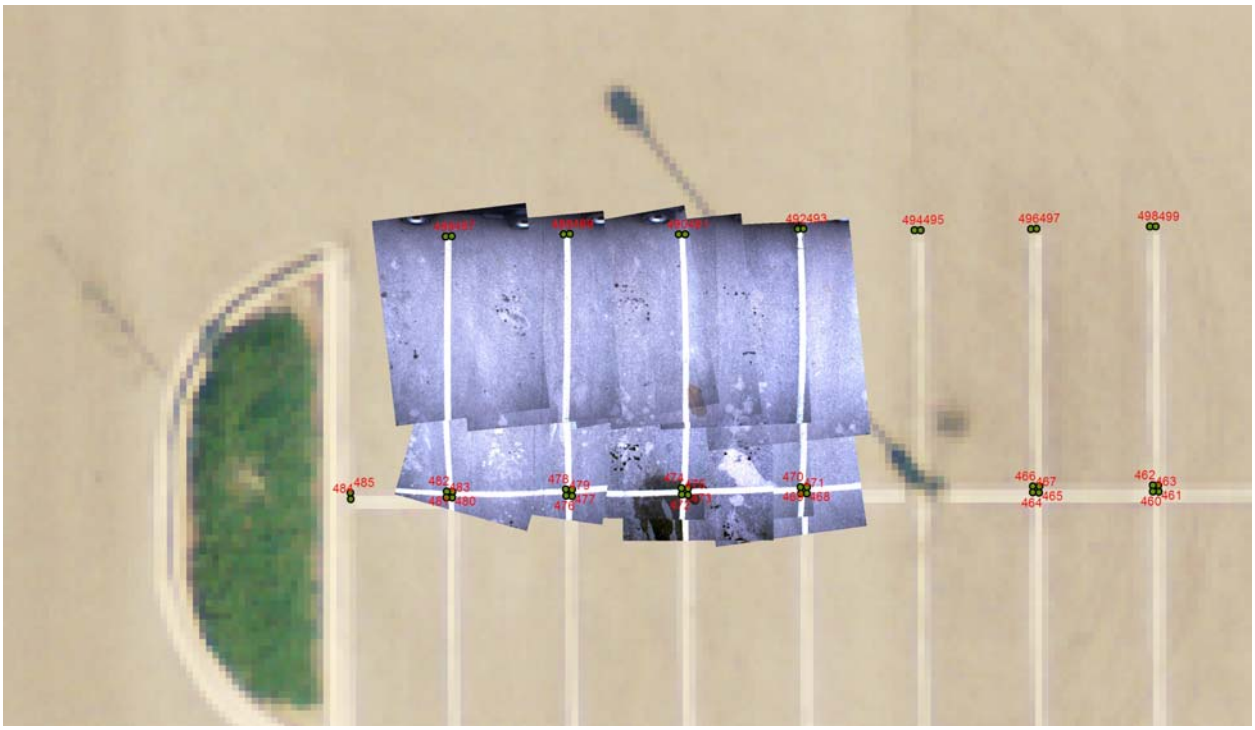

Figure C-1. Boresight calibration GCPs (background image from Alachua County Property Appraiser, foreground images by author)

LIST OF REFERENCES

Allan, David W., Neil Ashby, Clifford C. Hodge 1997. The Science of Timekeeping. Hewlett Packard Application Note 1289.

Alkan, R. M. 2009. Development of a low-cost positioning system using OEM GPS receivers and usability in surveying applications. FIG Congress 2010.

Benjamin, Adam, Benjamin Wilkinson, Ahmed Mohamed. 2010. seqori ..SaLIS paper, accepted for publication, *Surveying and Land Infromation Science*, 40(3).

Briscoe, John. 1983. The use of tidal datums in the law. *Surveying and Mapping*, 43(2): 115-121.

Butgereit, Richard. 2009. Regional evacuation studies with analysis of storm surge – update. Florida State Emergency Response Team. http://www.floridadisaster.org/GIS/LiDAR/Documents/project_status_20090120.pdf

Center for Operational Oceanographic Products and Services. 2000. “Tidal Datums and their Applications”. Silver Springs, MD.

Clough, Jonathan S., Richard A. Park, and Roger Fuller. 2010. “SLAMM 6 bete Technical Documentation”, Warren Pinnacle Consulting, Inc.

Cole, George M. 1997 *Water Boundaries.* John Wiley & Sons, Inc. New York, NY.

Doyel, Thomas W., Ken W. Krauss, William H. Conner, and Andrew S. From. 2010. Predicting the retreat and migration of tidal forests along the northern Gulf of Mexico under sea-level rise, Forest Ecology and Management, 259:770-777

Dicks, Steve. 2006. Large-format imagery enhances LiDAR accuracy. *Earth Imaging and Remote Sensing.* March 2006.

DiGruttolo, Nicholas. and Ahmed Mohamed. 2010. seqori ..SaLIS paper, accepted for publication, *Surveying and Land Infromation Science*, 40(3).

E-con Systems. 2005. “e-con’s Spark Kit PRODUCT SPECIFICATION”.

Federal Emergency Management Agency (FEMA). 2003. “Guidelines and Specifications for Flood Hazard Mapping Partners, Appendix A: Guidance for Aerial Mapping and Surveying” www.fema.gov/library.

Fischman, Robert L. 1991. Global warming and property interests: preserving coastal wetlands as sea levels rise. *Hofstra Law Review,* 19 Hofstra L. Rev. 565

Florida Department of Environmental Protection, Bureau of Survey and Mapping (FDEP). 2003. “Tide Methodologies” accessed July 31, 2008 http://data.labins.org/2003/SurveyData/WaterBoundary/MHW/documents/TideMethodologies.pdf

Florida Sea Grant. 2010 “Ecosystem Health”, 19 May 2010, http://www.flseagrant.org.

Fuji Film. 2010. Fujion product data sheet.

Gibson, David W. 2010. Personal communication. Associate Emeritus Professor, Geomatics Program, University of Florida.

Intergovernmental Panel on Climate Change (IPCC). 2007. “Climate Change 2007: Synthesis Report”, pg. 30

Intergovernmental Panel on Climate Change (IPCC). 2008. “Climate Change and Water”, IPCC Technical Paper VI, pg. 28.

Knight, Jon M., Pat E.R. Dale, John Spencer, Lachlan Griffin. 2009. Exploring LiDAR data for mapping the micro-topography and tidal hydro-dynamics of mangrove systems: An example from southeast Queensland, Australia. *Estuarine, Coastal and Shelf Science*, 85:593-600.

Magellan International. 2007 “AC12 Receiver” product data sheet.

Marmer, H. A.. 1951 “Tidal Datum Planes”, U.S. Government Printing Office, Washington.

Memsense. 2008 “nIMU Nano Inertial Measurement Unit Series Documentation”.

Microdrones. 2010. Microdrones GmbH website, md4-1000 technical data page. http://www.microdrones.com/en_md4-1000_tech_data.php.

Morril, John B. and James P. Herbert. 1990. “Midnight Pass Position Paper”. The Midnight Pass Society, Inc.

National Oceanic and Atmospheric Administration (NOAA). 2010a. “Estimation of Vertical Uncertainties in Vdatum”. http://vdatum.noaa.gov/docs/est_uncertainties.html.

National Oceanic and Atmospheric Administration (NOAA). 2010b. “Mean Sea Level Trend 8727520 Cedar Key, Florida”. http://tidesandcurrents.noaa.gov/sltrends/sltrends_station.shtml?stnid=8727520 Cedar Key, FL.

National Oceanic and Atmospheric Administration (NOAA). 2010c. “A Tutorial on Datums”. http://vdatum.noaa.gov/docs/datumtutorial.html.

Parker, B., Milbert, D. G., Wilson, R., Hess, K. W., Bailey, J., Berry, R., Fowler, C., Gesch, D. 2001. A Tampa Bay bathymetric / topographic digital elevation model with internally consistent shorelines for various datums. *Proceedings of the Twelfth Biennial International Symposium of the Hydrographic Society*, University of East Anglia, Norwich, UK: 11-11 through 11-11.

Pilkey, Orrin H., and Katharine L. Dixon. 1996. *The Corps and the Shore*, Island Press, Washington, DC. Pg 14.

Pinchin, James, Chris Hide, David Park, and XiaoQi Chen. 2008. "Precise kinematic positioning using single frequency GPS receivers and an integer ambiguity constraint", ION Position, Location and Navigation Symposium, http://www.jamestpinchin.com/Publications/Pinchin_PLANS08.pdf.

Pokharel, Parameshor, Makoto Takeda, and Matsuo Naoki. 2009. Inundation analysis in the coastal area considering climate change due to global warming. *Water, Air, & Soil Pollution: Focus*, 9:393-401.

Point Grey Research. 2010. Chameleon "Getting Started", technical specifications.

Pugh, David T. 1996. *Tides, Surges and Mean Sea-Level.* John Wiley and Sons, Chichester, U.K.

Quandros, Nathan D. and Philip A. Collier. 2008. A new approach to delineating the littoral zone for an Austrailian Marine Cadastre. *Journal of Coastal Research*, 24(3):780-789.

Sax, Joseph L. 2010. Some unorthodox thought about risin sea levels, beach erosion, and property rights. *Vermont Journal of Environmental Law,* 11 Vt. J. Envtl. L. 641.

Schleppe, John B. 2006. "Interface and Performance Evaluation of u-blox LEA-4T (Antaris4 Chipset) for Attitude Determination Using HEADRT+TM", Position, Location and Navigation Group, Department of Geomatics Engineering, University of Calgary, 30 June, 2006.

Schurman, P. 1941. "Manual of Harmonic Analysis and Prediction of Tides, Special Publication No. 98". U.S. Government Printing Office, Washington.

Skaloud, Schaer P. 2003. "Towards a More Rigorous Boresight Calibration". Swiss Federal Institute of Technology Lausanne (EPFL).

Solinst. 2010. "Levelogger Series Model 3001 Data Sheet".

Thompson, Douglas A. 2000. "Tidal Boundaries: A Surveyors Responsibility". Atlantic Professional Development.

Titus, James G. 2009. “Coastal Sensitivity to Sea-Level Rise: A Focus on the Mid-Atlantic Region”, U.S. Climate Change Science Program, Synthesis and Assessment Product 4.1, http://www.epa.gov/climatechange/effects/coastal/sap4-1.html.

Traugott, J., B. Braun, F. Holzapfel, and G. Sachs. 2009. Precise kinematic relative positioning with a stand-alone miniaturized L1 GPS data logger. *NATO Research and Technology Organisation*, <ftp.rta.nato.int/public//PubFullText/RTO/EN/...///EN-SET-116-06.doc>.

UAS. 2010. UAS website homepage. http://uav.ifas.ufl.edu/home.html.

U-blox. 2010. “ANN-MS Data Sheet”, http://www.u-blox.com/images/downloads/Product_Docs/ANN_Data_Sheet%28GPS-X-02021%29.pdf.

United States. 2007. “Climate change agencies should develop guidance for addressing the effects on federal land and water resources: report to Congressional requesters”, Washington, D.C.: U.S. Govt. Accountability Office. http://www.gao.gov/new.items/d07863.pdf.

Waegli, Adrian and Jan Skaloud,. 2009. Optimization of two GPS/MEMS-IMU integration strategies with application to sports. *GPS Solutions*, 13:315-326.

Wiechert, Alexander and Michael Gruber. 2009. Photogrammetry versus lidar: clearing the air. *Professional Surveyor Magazine*, Aug. 2009.

Wolf, Paul R., and Bon A. Dewitt. 2000. *Elements of Photogrammetry with Applications in GIS*. McGraw-Hill. Boston, MA.

Woodworth, P.L., F.N. Teferle, R.M. Bingley, I. Shennan, and S.D.P. Williams. 2009. Trends in UK mean sea level revisited. *Geophysical Journal International*, 176:19-30.

BIOGRAPHICAL SKETCH

Nicholas DiGruttolo was born in Sarasota, Florida. He graduated from New Directions High School in 1988 and began a career in land surveying. He remained in Sarasota until 2006 where he worked for the Cadastral Surveying Section of the county government for over 15 years. After completing an A.A. at Manatee Community College in the evenings he resigned his position with the county to pursue a B.S. in geomatics at the University of Florida.

Upon graduating in May 2008, Nicholas obtained licensure as a Professional Surveyor and Mapper with the State of Florida and began working for Northrop Grumman Corporation. As a Field Engineering Services Manager, Nicholas coordinates survey projects in remote locations throughout the world and has personally worked in 12 states and three foreign countries.

Living in Florida for his entire life gave Nicholas a great appreciation for the coastal environment and influenced him to focus his efforts in pursuit of a M.S. on coastal issues that impact property rights. Upon completion of the M.S. Nicholas will continue his education at the University of Florida and employment with Northrop Grumman.

Nicholas has been married for 10 years to Laura and they have two children, Lucas, age 6; and Brody, age 4. Laura encourages Nicholas to continue his education and provides the stability at home to allow him to be successful while also continuing her career as an ecologist.